DOI: 10.1002/adhm.201600164
Article type: Full Paper

Metabolic characteristics of 16HBE and A549 cells exposed to different surface modified gold nanorods

Zhigang Liu, Liming Wang, Limin Zhang, Xiaochun Wu, Guangjun Nie, Chunying Chen, Huiru Tang, Yulan Wang**

Z. Liu, Dr. L. Zhang, Prof. Y. Wang
CAS Key Laboratory of Magnetic Resonance in Biological Systems, State Key Laboratory of Magnetic Resonance and Atomic and Molecular Physics, Wuhan Centre for Magnetic Resonance, Wuhan Institute of Physics and Mathematics, University of Chinese Academy of Sciences, Wuhan, 430071, China
E-mail: yulan.wang@wipm.ac.cn

Dr. L. Wang, Prof. X. Wu, Prof. G. Nie, Prof. C. Chen
CAS Key Laboratory for Biomedical Effects of Nanomaterials and Nanosafety, CAS Center for Excellence in Nanoscience, National Center for Nanoscience and Technology and Institute of High Energy Physics, Beijing, 100190, China

Prof. H. Tang
State Key Laboratory of Genetic Engineering, Biospectroscopy and Metabolomics, School of Life Sciences, Fudan University, Shanghai, 200433, China
Email: huiru_tang@fudan.edu.cn

Prof. Y. Wang
Collaborative Innovation Center for Diagnosis and Treatment of Infectious Diseases, Hangzhou, 310058, China

Keywords: Gold Nanorods; Metabolomics; Biomedical Applications; Surface Modification; Cancer Cell

Gold nanorods (AuNRs) have shown their great potential in cancer treatment due to their special physiochemical and optical properties, and the ease of surface modification. However, the molecular mechanism of biological effects induced by different surface modified AuNRs remains largely undetermined. Herein, we for the first time systematically analyzed metabolic impacts of three surface modified AuNRs in cancer and non-cancer cells detected by NMR and GC-FID/MS metabolomics and validated by molecular biological approach. We found that positively and negatively charged AuNRs induced different metabolic consequences. Most importantly, we found that the PEI-AuNRs displayed specific cytotoxicity to A549 cells whilst posing little impact on 16HBE cells. The cytotoxicity of PEI-AuNRs to A549 cells is

manifested in large disruptions to the cell metabolisms, which affects energy metabolism, choline metabolism, the hexosamine biosynthesis pathway and oxidative stress to cells. Our results provided comprehensive molecular information on the distinct biological effects of different surface modified AuNRs, and could be valuable in designing purpose-driven nanomaterials. Most importantly, this work highlighted the potential of metabolomics coupled with molecular biological techniques in screening anti-tumor nanodrugs and revealing the molecular mechanism of their biological effects.

1. Introduction

Biomedical nanomaterials are less than several hundred nanometers in size, very similar to the size of large biological molecules, such as enzymes and antibodies. These nanoparticles are anticipated to interact with various kinds of biological molecules, for instance, proteins and receptors both on the surface and inside of cells.[1] Hence, nanoscaled materials for medical use have gained increasing attention in recent years. Among those materials, gold nanorods (AuNRs) are especially attractive due to their special physiochemical and optical properties, as well as the ease of modification with various coating surfaces. In recent years, AuNRs have been widely researched in drug and gene delivery, molecular imaging and cancer photothermal therapy.[2-4]

Despite the potential application of AuNRs in the biomedical field, increasing attention has been paid to the safety issues of AuNRs. It is well established that AuNRs synthesized with CTAB (cetyltrimethylammonium bromide) is toxic as CTAB can cause mitochondria dysfunction, leading to apoptosis.[5] Therefore, replacements or modifications to CTAB have been proposed. PEG (polyethylene glycol) has been developed initially for better biocompatibility, water solubility, decreased enzymatic degradation, and non-immunogenicity.[6] However, adverse effects to liver cells including inflammation and apoptosis, were associated with PEG-coated gold nanoparticles.[7] In recent years, poly

sodium-p-styrene sulfonate (PSS)-AuNRs, poly diallyldimethyl ammonium chloride (PDDAC)-AuNRs and branched poly ethylenimine (PEI)-AuNRs have been developed. It is reported that toxicity of additional coatings of PSS or PDDAC to CTAB coated AuNRs were largely reduced.[5] PSS-AuNRs are anionic, whereas PDDAC-AuNRs and PEI-AuNRs are cationic. It is worth noting that properties of surface molecules and charges on the surface of AuNRs are expected to interact with cells in different ways. Previous studies have shown that cationic nanoparticles could improve delivery of drugs to cells, while anionic nanoparticles diffuse much faster, hence delivering drugs deeper into tissues because anionic nanoparticles repel negatively charged cell membrane.[8] The positively charged AuNRs also adsorb more proteins on their surface and are distributed in the outer region of the tissues, whereas negatively charged coatings have better penetration ability and are homogeneously distributed inside tissues.[9] Thus, the charges of AuNRs will ultimately affect their biological function within cells.

Surface modified AuNRs could be used as drug carriers to improve the performance of a drug and reduce drug toxicity. Hauck *et al.* reported that PDDAC-AuNRs heated together with cisplatin lowered the cytotoxic drug dosage requirements to roughly 1/3 of the unheated amount.[10] Rejiya *et al.* further demonstrated that PSS-coated AuNRs conjugated with EGFR antibody could induce cell death in 90% of carcinoma cells, when coupled with laser treatment.[11] In addition to photothermal therapy, these AuNRs can also be used as transfection reagents. Lee *et al.* studied positively charged PEI-coated AuNRs for siRNA delivery and found that PEI-AuNRs could form stable complexes with siRNA, which resulted in a gene silencing effect in cancer cells.[12] *Xu et al.* also demonstrated that PDDAC-AuNRs and PEI-AuNRs might act as DNA vaccine adjuvants to treat HIV as HIV-1 Env plasmid DNA could be delivered to host cells by these two modified AuNRs to enhance immunity.[13] Although these surface modifications have shown potential application in nanomedicine, comprehensive biological impact and toxicity of these materials have yet to be fully

elucidated. Understanding the underlying relationship between the biological effects and different surface coatings could provide vital information for designing purpose-driven nanomaterials.

Recently, researches on the interaction between AuNRs and proteins using proteomics have opened a window for omics investigation on biomedical nanomaterials.[14, 15] The metabolome is deemed to be much more closely linked to phenotype than the proteome or transcriptome.[16, 17] Therefore, to further elucidate the metabolic effects of AuNRs exposure to an organism, metabolomics could be applied. Our previous studies have demonstrated the suitability of the metabolomics technique in deriving endpoint biological effects of nanomaterials.[18, 19] In this investigation, we aimed to investigate the biological effects of different surface coated AuNRs, namely, PSS-, PDDAC- and PEI-AuNRs, by observing the metabolic changes in both lung cancer cells (A549) and non-cancer cells (16HBE, derived from normal human bronchial epithelial cells and commonly used as non-cancer lung cells in researches) exposed to these AuNRs. We for the first time systematically investigated the time and surface chemistry dependent metabolic alterations in both normal and tumor cell extracts and cell culture media after exposure to different-polymer-coated AuNRs and validated our results at the transcriptional level using Real-Time PCR. We found that the PEI-AuNRs displayed specific cytotoxicity to A549 cells whilst posing little impact on 16HBE cells. The major metabolic alterations associated with the cytotoxicity are disruptions of energy metabolism, choline metabolism, hexosamine biosynthesis pathway (HBP), and induced oxidative stress to cells. Our results provided detailed picture of the metabolic impact of different surface coated AuNRs, and established a relationship between these different coated AuNRs and biological effects they induced. This information would be useful in designing purpose-driven nanomaterials.

2. Results

2.1. Characterization, cytotoxicity and cellular uptake of different coated AuNRs.

Different surface coated AuNRs were prepared as described previously.[13, 20] As-prepared AuNRs are coated with CTAB bilayers and exhibit positive surface charge. The average particle size was obtained by measuring more than 100 nanorods in TEM (**Figure S1**). The CTAB-AuNRs had a mean aspect ratio of 4.2 with a mean length of 55.7 ± 7.6 nm and width of 13.2 ± 1.7 nm. Layer by layer modification was used to produce differently coated AuNRs, i.e., PSS was coated onto CTAB-AuNRs via electrostatic adsorption to form negatively charged PSS-AuNRs; PSS-AuNRs were further coated with PDDAC or PEI to form positively charged PDDAC-AuNRs or PEI-AuNRs, respectively (**Figure 1** A-D). As all different surface coated AuNRs came from the same batch, they have same geometric sizes with as-prepared CTAB-coated ones. The surface charge of the AuNRs was determined by measuring the zeta potential. These surface modified AuNRs have similar UV-vis-NIR spectra with a longitudinal surface plasmon resonance peak of approximate 800 nm (Figure 1 E).

We then performed the live-dead assay to evaluate the cytotoxicity of the three different AuNRs. Cells were treated with 50 μM of AuNRs (final concentration in the culture medium based on Au atoms) for 12 h, 24 h or 48 h, and stained with a live-dead assay. This concentration 50 μM AuNRs was optimal to attempt metabolism and gene expression without too much toxicity to cells according to our previous report.[21] During confocal microscopy, live cells fluoresced green, while dead cells were red (**Figure S2**). Incubating with 50 μM of all AuNRs caused deformation and cell death of A549 cells at 12 h , whilst normal 16HBE cells remained intact. Continuous incubating for 24 h and 48 h resulted in a greater number of dead A549 cells as compared with 16HBE cells (Figure 1 F). PEI coated AuNRs caused most cell death in A549 cells, followed by PSS and PDDAC. These observations suggested that these AuNRs were toxic to A549 cells with PEI-AuNRs in particular. Sporadic cell death was

observed at 24 h and 48 h when 16HBE cells were exposed to AuNRs, suggesting that AuNRs have slight cytotoxicity to non-cancer 16HBE cells.

Then we used confocal microscopy to investigate the localization of PEI-AuNRs in cells. We found few PEI-AuNRs in 16HBE cells after exposure for 1h; continuous treatment of 3-6 h, more PEI-AuNRs were taken up by 16HBE cells (Figures S3 & S4, Supporting Information). Noticeable amount of PEI-AuNRs were found in lysosome at 12 h of exposure and few were found in mitochondria at 24 h of incubation. In contrast to 16HBE cells, A549 cells took up PEI-AuNRs more quickly (Figures S5 & S6, Supporting Information). Most of PEI-AuNRs already distributed in lysosome at 6 h of exposure. Similar to 16HBE cells, few PEI-AuNRs entered mitochondria. We also used dark field microscopy to confirm these results (Figure S7, Supporting Information). We found that cellular uptake of PEI-AuNRs were scarce for both cells after 3 h of treatment. However, strong lumination noticed at 12 h incubation suggested substantial uptake of PEI-AuNRs by cells.

2.2. Metabolic profiles of AuNRs treated A549 and 16HBE cells and cell culture media

A total of 60 metabolites from different metabolic pathways were identified in high resolution one dimensional ^{1}H NMR spectra from A549 and 16HBE cell extracts and cell culture media (**Figure 2**). The resonance peak assignment shown in **Table S1** was facilitated by published literature and confirmed by a series of two dimensional NMR spectra including ^{1}H J-resolved, ^{1}H–^{1}H TOCSY, ^{1}H–^{1}H COSY, ^{1}H–^{13}C HMBC and ^{1}H–^{13}C HSQC.[22, 23] The NMR spectra were chiefly composed of resonance peaks from a number of amino acids, amino sugar, glucose, organic acids, such as lactate and creatine, nucleotides and nucleosides, such as guanosine, uracil, inosine, nicotinamide adenine dinucleotide (NAD^{+}), and membrane metabolites, such as choline, phosphocholine (PCho), glycerophosphocholine (GPC).

2.3. Impact of different AuNRs on metabolic profiles of cells

We employed multivariate data analysis to analyze the time and surface dependent cellular responses induced by different surface coated AuNRs. Principal component analysis (PCA) was used to observe the global metabolic profiles of all the groups obtained at 12 h post exposure. We observed a metabolic difference between cells treated with negatively and positively charged AuNRs (**Figure 3**). This observation suggested that the charges of AuNRs play a role in altering the metabolic profile in cells. In addition, A549 cells treated with PDDAC-AuNRs showed a similar metabolic profile compared with that of the untreated cells. In contrast, PEI- and PSS-AuNRs treated A549 cells were clearly metabolically different from those of PDDAC-AuNRs treated and the untreated A549 cells, suggesting that PEI- and PSS-coated AuNRs profoundly disrupted cancer cell metabolism.

We then constructed an orthogonal projections to latent structures - discriminant analysis (OPLS-DA) model to compare the metabolic profiles of 16HBE cells treated by both positively and negatively charged AuNRs. OPLS-DA is a multivariate data analysis tool that is commonly used to differentiate the metabolic profiles of two groups.[24] The model was also cross validated with coefficient of variation - analysis of variance (CV-ANOVA) and permutation tests. The color-coded coefficients generated from the models were plotted with loadings in **Figure 4**. In this plot, the abscissa is chemical shift, representing metabolites. The absolute value of coefficient (r) indicates the significance of altered metabolites with red color more significant than the blue color. The concentrations of alanine, succinate, choline and uracil in 16HBE cells treated with negatively charged AuNRs were higher than those in 16HBE cells treated with positively charged AuNRs, while the concentrations of fumarate, guanosine, UDP-N-Acetyl glucosamine (UDP-GlcNAc), UDP-N-Acetyl galactosamine (UDP-GalNAc) were lower in 16HBE cells treated with negatively charged AuNRs (Figure 4 A&B). These metabolites derived from glucose metabolism, choline metabolism and nucleotide metabolism underlined that positive and negative surface charges resulted in different metabolic disruptions to 16HBE cells.

It is also interesting to note that the two positively charged AuNRs caused different metabolic reposnses of cells (Figure 3). We further compared metabolic profiles of A549 cells treated by PDDAC-AuNRs and PEI-AuNRs for 12 h duration using OPLS-DA strategy (Figure 4 C). We found that exposure to PEI-AuNRs led to decrease of all metabolites that can be observed in NMR spectra. This observation suggested that PEI-AuNRs caused specific impact to A549 cells.

2.4. A549 and 16HBE cells respond differently to AuNRs exposure

In order to evaluate metabolic effects of different surface charged AuNRs on A549 cancer cells and on normal 16HBE cells, comparisons were made between AuNRs exposed cells and corresponding untreated cells at matched time points using OPLS-DA (Figure S8). Except for PEI-AuNRs treated A549 cells which showed an irreversible decrease of a large quantity of metabolites, most treated cells demonstrated a recovery of down-regulated metabolites when treated for 24 h and 48 h, which reflected cells self-regulating to the stress of AuNRs. Since metabolic alterations occurred well before cell death, we plotted alterations of metabolites at 12 h to illustrate metabolic consequences induced by these AuNRs (**Figure 5**). We observed that these AuNRs treatments resulted in depleted levels of a wide range of metabolites at 12 h of incubating with AuNRs, e.g. energy related metabolites, lactate and succinate, choline metabolites, GPC, most amino acids, such as valine and threonine. Besides, decreased levels of HBP metabolites, UDP-GlcNAc and UDP-GalNAc, oxidative stress relative metabolites, glutathione (GSH), pentose phosphate pathway metabolites, NAD^+ and $NADP^+$ were also detected. In addition, several metabolites were elevated after AuNRs treatment. For instance, the levels of glucose, fumarate, lysine and inosine-5'-monophosphate (5'-IMP) increased in PEI-AuNRs treated 16HBE cells. Among these treatment groups, PEI-AuNRs induced the largest number of metabolic disruptions to A549 cells while few changes were trigged to 16HBE cells. PDDAC-AuNRs induced the fewest metabolic changes to A549 cells, whereas

PSS-AuNRs induced comparable changes between normal 16HBE cells and A549 cancer cells. Independent measurement of GSH/GSSG also showed a rapid drop in the ratio of GSH/GSSG in A549 cells treated with PEI-AuNRs compared to few changes observed in 16HBE cells (Figure 5 I).

2.5. GC-FID/MS analysis of fatty acid composition

Interaction between AuNRs and cells occurs through the cell membrane, of which fatty acids are a major component, therefore, changes in fatty acids were anticipated to associate with treatment of different coated AuNRs. A total of 19 fatty acids were identified and quantified, which were C14:0, C16:0, C18:0, C20:0 and their corresponding unsaturated forms (**Figure 6**). Compared with the untreated cells, AuNRs resulted in a largely increase in the levels of fatty acids in A549 cells at 12 h of treatment whilst few changes were noted in 16HBE cells.

2.6. The transcriptional levels of certain genes in the altered metabolism

In order to validate the metabolic alterations observed using metabolomics, particularly metabolisms related to energy metabolism, oxidative stress and membrane turnover, mRNA expression levels of key enzymes were also determined by quantantive RT-PCR. As shown in **Figure 7**, the expression of *GCLC*, *GSS* and *GSR*, which encode the enzymes in the GSH anabolic pathway, were upregulated in AuNRs treated A549 cells. Moreover, an altered expression of *CHKA* in both cell types exposed to AuNRs was also observed (Figure 7). As *CHKA* encodes the enzyme that catalyzes choline to phosphocholine (PCho), the first reaction in the CDP-choline cycle, our results suggested a disruption in the membrane function.[25] Interestingly, the expression of phosphocholine cytidylyltransferase A (*PCYT1A*) that controls the rate-limiting reaction in the CDP-choline pathway, significantly increased in AuNRs treated A549 cells, but decreased in AuNRs treated 16HBE cells. The expression of glutamine-fructose-6-phosphate amidotransferase (*GFPT1)* that controls the rate-limited

enzyme in the HBP, was depleted in AuNRs treated 16HBE cells (Figure 7), which was consistent with reduced levels of end products of hexosamine pathway (e.g. UDP-GalNAc, UDP-GlcA, UDP-Glc and UDP-GlcNAc) in cells treated with AuNRs. The downregulated hexosamine pathway was also consistent with reduced expression of *OGT* (Figure 7), which controls the enzyme *O*-GlcNAc transferases during O-GlcNAcylation.

3. Discussion

Decades of researches on cancer therapy have resulted in the development of a number of anti-tumor drugs with different mechanisms. Gold nanorods (AuNRs) are at the forefront of the researches due to their potential as a drug carrier and putative role in cancer photothermal therapy. AuNRs can be modified with various coating surfaces, which results in different biological properties and biological functions. In this study, we investigated the effects of AuNRs coated with different materials, namely PSS, PDDAC and PEI, and used metabolomics to observe the resulting metabolic changes in both lung cancer cells and normal cells exposed to these AuNRs. In addition, we validated some important pathways using molecular biological technique.

3.1. Different surface charges induce distinct metabolic alterations

In this investigation, we found an unambiguous difference in the metabolic profiles from negatively and positively charged AuNRs treated 16HBE cells, which demonstrated that surface charge may influence the interaction between AuNRs and cells. It is reported that AuNRs could absorb serum proteins at contacting cell medium, forming so-called protein corona.[1] Therefore protein corona interacts with cells directly. However, the surface chemistry and charges of AuNRs affect the kinds of proteins that the AuNRs may absorb, thereby affect uptaking and distribution of AuNRs in cells. Previous studies have shown that cells treated with positively charged AuNRs displayed a more overt disruption of plasma

membrane integrity, more severe lysosomal and mitochondrial injury, and a larger number of auto-phagosomes, as compared with cells treated with negatively charged AuNRs.[26] In our study, we found that glucose metabolism through pyruvate was up-regulated in cells treated with negatively charged PSS-AuNRs, which was manifested in the increased levels of lactate, TCA cycle intermediate, succinate and alanine (Figure 4, Figure 5). In addition, the pentose phosphate pathway shifted towards producing more of uracil in cells treated with negatively charged AuNRs. Furthermore, increased levels of fatty acids (Figure 6) together with the decreased levels of choline in A549 cells treated with positively charged AuNRs (Figure 5) suggested the down-regulation of choline metabolism associated with treatment of positively charged AuNRs. Increased choline metabolism is deemed as a metabolic hallmark associated with oncogenesis and tumor progression.[27] Exposure to positively charged AuNRs could be used as an efficient way to down-regulate choline metabolism of cancer cells.

There are substantial differences in the metabolic response of cells treated by PDDAC-AuNRs and PEI-AuNRs although both are positively charged, which suggested that strucutre of the coating has biological impact on cells. It is reported that cationic nanoparticles affect cells through a polycation-mediated endocytosis, a three-step process composed of binding with phospholipids and/or glycolipids in the membrane, internalization into cells, and exit from the endosome.[28] However, as each surface molecule has its unique structure, the interaction with cells could be different. It is reported that PEI is cytotoxic by two different mechanisms: the disruption of the cell membrane leading to necrotic cell death (immediate) and disruption of the mitochondrial membrane after internalization leading to apoptosis (delayed).[29] In our confocal microscopy experiment, we found that PEI-AuNRs mainly located in the lysosome. And we observed abnormal choline metabolism due to the exposure of PEI-AuNRs detected by metabolomics. These results reflected that the main toxicity may be caused by the interaction of PEI-AuNRs with cell membrane. Furthermore, every third atom in PEI structure is a protonated nitrogen, which contributes to its large buffering

capacity known as proton sponge effect.[30] However, the large amount of positive charges induce strong interaction with cell membrane, which leads to cell death. As for PDDAC, no obvious cytotoxicity was reported until now.[5] While for 16HBE cells, we previously demonstrated that AuNRs were translocated to endosomes/lysosomes after they entered 16HBE cells, and they remained there for some time till excluding from the cells, and 16HBE cells were more able to cope with the stress induced by AuNRs than A549 cells.[21] This may explain why the two positively charged AuNRs cause similar effects to 16HBE cells.

3.2. Different metabolic responses of 16HBE and A549 cells to AuNRs exposure

We demonstrated that three of the AuNRs caused more cell death in A549 cells as compared with 16HBE cells. This is particularly true for PEI-AuNRs since our cytotoxicity assay has demonstrated that PEI-AuNRs caused most of cell death for A549 cells while posed little effects on 16HBE cells. In addition, this observation was also echoed by the metabolic effects of PEI-AuNRs, as we observed significant metabolic disruptions in A549 cells exposed to PEI-AuNRs and minor disruptions to 16HBE cells. These disruptions included metabolites involved in pathways of glucose metabolism, and metabolic pathways involved in phospholipid synthesis and oxidative stress (**Figure 8**).

Firstly, the impact of different AuNRs on A549 cells and 16HBE cells was manifested in glycolysis metabolism. In our investigation, we found the level of glucose in the culture media of PEI-AuNRs treated A549 cells was higher than that in the control group (Figure S9). The low consumption of glucose indicated the inhibition of glucose metabolism of A549 cells. Concurrently, the decreased level of lactate in A549 cells was induced by PEI-AuNRs exposure, which indicated that PEI-AuNRs inhibited the intracellular anaerobic glycolysis. This observation is consistent with previous investigations that show AuNRs modulate the micro-environment of tumor cells by inhibiting lactate dehydrogenase (LDH).[18] In addition,

metabolites in TCA cycle such as succinate also decreased in cells treated with PEI-AuNRs, which implied that PEI-AuNRs caused mitochondrial dysfunction and inhibited the energy metabolism of A549 cells. This observation is in accordance with the finding that PEI activates a mitochondrial mediated apoptosis.[29] Our observation of lowest viability for PEI-AuNRs treated A549 cell provided supportive evidence for disruption of the mitochondrial function. In PDDAC-AuNRs and PSS-AuNRs treated cells, we also found a decrease in energy metabolism related metabolites, such as succinate, which reflected that these AuNRs commonly inhibited the energy metabolism of cells. The difference between these AuNRs lies in the degree of their impact.

Secondly, different impact of AuNRs on A549 cells and 16HBE cells was also manifested in the HBP. The HBP plays a vital role in the nutrient signaling in mammalian cells. UDP-GlcNAc and UDP-GalNAc are generated from glucose via the HBP and act as donor molecules for glycosylation of lipids and proteins, which is important in lots of biological processes and diseases including cancer.[31, 32] The level of UDP-GlcNAc is a vital factor in the production of β1,6-branched oligosaccharides that are closely associated with tumor progression and metastasis.[33] The depletion of UDP-GlcNAc leads to downstream events culminating in cell death.[34] In our investigation, we found apparent decreases of UDP glucuronate (UDP-GlcA), UDP-GalNAc and UDP-GlcNAc in A549 cells after exposure to PEI-AuNRs. This is again consistent with the lowest viability for PEI-AuNRs treated A549 cells, suggesting potential of PEI-AuNRs in cancer research.

Thirdly, the impact of different AuNRs on A549 and 16HBE cells was also reflected in the phospholipid synthesis. In this investigation, the levels of PCho and GPC decreased in most of the AuNRs-treated groups, in which PEI-AuNRs treated A549 cells reduced the most. This observation suggested that phospholipid synthesis was inhibited by AuNRs treatment. This

change was associated with marked increase in the levels of fatty acids (e.g. C20:4n6, C18:2n6, C18:1n9, C18:0, C16:0) in AuNRs treated cells, which suggested increased catabolism of phosphatidylcholine (PC) as fatty acids and choline derivatives are the main components of membrane phospholipid bilayer. When AuNRs contact the cell membrane, they can be recognized by cells, thus triggering a series of responses such as uptake, translocation, accumulation, exclusion and cell death.[5, 21] It is widely recognized that abnormal choline metabolism is a phenotype of cancer and recent researches emphasize the complex reciprocal interactions between oncogenic signaling and choline metabolism.[27] The increase of choline and its derivatives were found in many tumor types, such as brain cancer and lung cancer.[35-38] Decreased phospholipid synthesis induced by AuNRs suggests that AuNRs have a significant potential for cancer therapy by targeting choline metabolism.

Finally, the impact of different AuNRs on A549 and 16HBE cells also was shown in the different capability of these treated cells in dispensing reactive oxygen species (ROS) that was known to be produced by AuNRs exposure.[39] ROS can induce damage to DNA and protein, and eventually lead to cell death, through the activation of transcription factors including AP-1, MAPK and NF-κB pathways.[40, 41] In this study, we found markedly diminished levels of GSH, and decreased ratio of GSH/GSSG in PEI-AuNRs treated A549 cells, together with decreased levels of GSH precursors, glutamate and glycine. Although the genes *GCLC*, *GSS* and *GSR* encoding the enzymes in the GSH anabolic pathway were upregulated to synthesize GSH so as to counteract the oxidative stress, a large amount of ROS led to vast consumption of GSH, which manifested in the decline of GSH in A549 cells. While in 16HBE cells, *GSTP1* that encodes the enzyme to catalyze GSH to conjugate to the AuNRs was upregulated significantly. These results demonstrated that 16HBE were more able to accommodate the oxidative stress derived from AuNRs, which has been observed previously.[18]

4. Conclusion

In this investigation, we employed a holistic approach of metabolomics to investigate the biological impact of AuNRs with different coating surfaces, including PEI, PDDAC and PSS. We found that positively and negatively charged AuNRs induced distinctly different metabolic alterations to both cell lines. In addition, these three AuNRs showed higher cytotoxicity to A549 cancer cells than 16HBE normal cells, with PEI-AuNRs resulting in the highest anti-tumor effects and largest metabolic disruptions to cancer cells. The metabolic disruptions are mainly manifested in energy metabolism, choline metabolism, HBP pathway and metabolism associated with oxidative stress. These findings provided a detailed insight into the mechanism of cell specific toxicity of AuNRs at a molecular level. Our data are valuable in designing anti-cancer drugs that exclusively kill cancer cells while posing least harm to normal cells. Furthermore, we have highlighted the usefulness of metabolomics in screening anti-tumor nanodrugs and revealing the molecular mechanism of their biological effects.

5. Experimental Section

Chemicals and synthesis of different coated AuNRs: Sodium borohydride ($NaBH_4$), cetyltrimethylammonium bromide (CTAB), hydrogen tetrachloroaurate (III) trihydrate ($HAuCl_4 \cdot 3H_2O$), silver nitrate ($AgNO_3$), L-ascorbic acid (AA), sodium sulfate (Na_2SO_4) and hydroxyethyl piperazine ethanesulfonic acid (HEPES) were obtained from Alfa Chemical (UK). D_2O (99.9% in D) and sodium 3-trimethlysilyl [2,2,3,3-D4] propionate (TSP-D4) were obtained from Cambridge Isotope Laboratories (Miami, USA). Fetal bovine serum (FBS), Dulbecco's modified Eagle's medium (DMEM), and L-glutamine were obtained from Thermo Fisher Scientific Incorporation (USA). Ethidium bromide, acridine orange, poly sodium-*p*-styrenesulfate (PSS, MW: 70,000), poly diallyldimethyl ammonium chloride (PDDAC, MW: 100,000, 20%) and branched polyethylenimine (PEI, MW: 25,000) were

purchased from Sigma-Aldrich (USA). Methanol, sodium chloride, hexane, K_2CO_3, $NaH_2PO_4 \cdot 2H_2O$ and $K_2HPO_4 \cdot 3H_2O$ (in analytical grade) were purchased from Sinopharm Chemical Reagent Co. Ltd. (Shanghai, China). H_2O_2 (MOS) and HNO_3 (BV-III) were purchased from the Beijing Chemical Reagents Institute. Human bronchial epithelial (16HBE) cells and human alveolar epithelial carcinoma (A549) cells were purchased from Cell Bank in Peking University Health Science Center (PUHSC) and the American Type Culture Collection (ATCC), respectively.

Different coated AuNRs were synthesized using a well-developed electrostatic layer-by-layer assembly approach.[42] First, CTAB-AuNRs were prepared according to a previous publication.[5] Then, PSS layer was first assembled to CTAB-AuNRs to obtain negatively charged nanorods. In brief, CTAB-AuNRs (12 mL) were centrifuged at 3200 g for 10 min, and the precipitate was dispersed in PSS aqueous solution (2 mg mL^{-1}, 12 mL, containing 6 mM NaCl) and magnetically stirred for 3 h, then it was centrifuged at 3000 g for 10 min, and the resulting precipitate was re-dispersed in deionized water. For further coating with PDDAC or PEI, the similar procedure was applied to PSS-AuNRs. The UV-Vis-NIR absorption spectra of these AuNRs were carried out with a TECAN microplate reader (Tecan, Durham, USA) (Figure 1). The bandwidth of the light source was 5 nm. All the spectra were subtracted background with baseline acquired from the absorption of deionized water.

Cell culture and exposure to AuNRs: Human alveolar epithelial carcinoma (A549) cells and normal human bronchial epithelial (16HBE) cells were cultured in DMEM medium (20 mL, containing 10% (v/v) fetal bovine serum). They were seeded at a density of 6×10^6 cells/dish onto a 15 cm diameter Petri dish and each group had ten replicates. After 24 h, different coated AuNRs (50 μM) were treated. Cells were collected after being exposed to AuNRs for 12 h, 24 h or 48 h. The cells were harvested by trypsinization at about 100% confluence and washed for three times with cold PBS, then stored at -80 °C until extraction. The control

group without AuNRs exposure was prepared in the same way. The cell culture media were collected and frozen in liguid nitrogen and then stored in -80 °C until metabolites extraction.

Sample preparation: All the frozen cell samples were homogenized in ice-cold water/methanol solution (1:2, v/v) and subjected to three freeze-thaw cycles, then sonicated in ice water for 15 min with a sonication program of 1 min power following 1 min stop. The supernatant was collected after centrifugation at 12000 g at 4 ℃ for 10 min. The remaining pellets were further extracted twice with the same procedure. The supernatants were pooled together and freeze-dried after removal of methanol in vacuum. The solid residues were weighed and individually dissolved into phosphate buffer (600 μL, 0.1 M, K_2HPO_4/NaH_2PO_4 and pD 7.4) containing 90% D_2O and 0.01% TSP-d4 to calibrate the chemical shift.[43] After vortexing and centrifugation (12000 g, 10 min, 4 °C), the supernatants (550 μL) were transferred into 5 mm NMR tubes. The cell culture media (1.6 mL) were added by methanol (3.2 mL) and placed in the ice for 30 min, followed by centrifugation at 3200 g for 10 min at 4 °C. The supernatant (4 mL) was lyophilized and stored at -80 °C until NMR analysis..

NMR spectroscopy: One dimensional ^{1}H NMR spectra of the cell extracts and culture media were acquired at 25 °C on a Bruker AVANCE III 600 MHz NMR spectrometer equiped with an inverse cryogenic probe (Bruker Biospin, Germany). The first increment of NOESY pulse sequence [RD-90°-t1-90°-tm-90°-ACQ] were recorded with a recycle delay (2 s) and mixing time (80 ms). Typically, the 90° pulse length was about 10 μs and 64 number of scan were recorded into 32768 data points with a spectral width of 20 ppm. In order to identify metabolites, two-dimensional NMR spectra including ^{1}H J-resolved, ^{1}H–^{1}H TOCSY, ^{1}H–^{1}H COSY, ^{1}H–^{13}C HMBC and ^{1}H–^{13}C HSQC for typical samples were acquired and processed with the similar parameters as previously described.[44]

Data processing and multivariate data analysis: Free induction decays were multiplied by an exponential window function with a 1.0 Hz line broadening factor prior to Fourier transformation. All spectra were phase and baseline corrected, and referenced internally to the peak of TSP at 0.00 ppm using Topspin (V3.1, Bruker Biospin, Germany). The concentration of metabolites was calculated by deconvolution of the NMR spectra and compared to the internal standard TSP, and then normalized to the wet weight of cells. Multivariate data analysis was performed using SIMCA-P+ 12.0 (Umetrics, Sweden). PCA was emplyed to examine group clustering and detect potential outliers. And OPLS-DA was further constructed using the unit-variance scaling and validated by a seven-fold cross-validation method and CV-ANOVA approach ($p < 0.05$).[24, 45] The loadings from the models were further back transformed with color-scaled correlation coefficients of metabolites and plotted using an in-house developed script in MATLAB 7.1 (The Mathworks Inc., Natick, USA).[46] In the loading plots, the color-coded correlation coefficients showed the variables contributed to the intergroup differentiation, with warmer color representing metabolites more significant contribution to the model than colder colored ones.

Fatty acids analysis: The methylesterification of fatty acids was accomplished as described previously.[47, 48] Briefly, cells (10 mg) were dissolved in methanol/hexane solution (4:1, v/v, 1 mL) with internal standard hexane solution (20 μL, containing 1 mg mL^{-1} heptadecanoate-methylester, 0.5 mg mL^{-1} tricosanoate-methyl ester and 2 mg mL^{-1} 2,6-di-tert-butyl-4-methyl phenol (Sigma-Aldrich, USA)), then the methylation reaction was started by addition of acetylchloride (100 μL). The reaction was kept for 24 h at 25 °C in the dark and stopped by addition of K_2CO_3 (2 mL, 6% water solution). The solution was extracted 3 times with hexane (200 μL). All the supernatants were mixed together and evaporated until dry, then kept for GC analysis.

The prepared sample was redissolved with hexane (50 μL). The analysis was performed with a Shimadzu GC-MS 2010 plus chromatography system (Shimadzu Scientific Instruments, Japan) equipped with a flame ionization detector and a DB-225 column (cut to 10 m, 0.1 mm ID, 0.1 μm film thickness) (Agilent, USA). The injection volume was 1 μL and the split ratio was 60:1. The injection port and detector temperatures were set to 230 °C. The column temperature program was as follows: temperature was held at 55 °C for 0.5 min, increased to 205 °C at the speed of 30 °C min^{-1}, held at 205 °C for 3 min, increased to 230 °C at the speed of 5 °C min^{-1}, and then held at 230 °C for 2.5 min. The identification of fatty acids was made by comparison with standard fatty acid methyl esters according to the retention time and also confirmed by MS analysis. The quantity of fatty acids was determined by the internal standard.

Live-dead assay: Live-dead viability and cytotoxicity assay was performed to distinguish live and dead cells. This kit provides a two-color fluorescence cell viability assay to distinguish live cells (green fluorescence) from dead ones (orange-red fluorescence). The cells were stained with the dyes and observed under a confocal microscope (Nikon A1 series, Japan).

Determination of the ratio of GSH to GSSG: Cells were seeded on 96 well plates and incubated with or without AuNRs in complete medium for 12 h, 24 h or 48 h, then the concentration of GSH and GSSG were detected using an assay kit (Beyotime, S0053) according to protocol provided by the manufacture. All the detection were performed in triplicates and the results were presented with the ratio of cellular GSH to GSSG.

Quantitative RT-PCR analysis: Total RNA was isolated using Trizol (Transgen Biotech, Beijing, China). Reverse transcription was carried out by using the First Strand cDNA Synthesis kit (Thermo Scientific, Rockford, USA). Real-Time PCR analysis was performed

using SYBR Green RT-PCR kit (AB systems). Gene transcription data were normalized to *GAPDH*. The primers are given in **Table S2**.

Intracellular localization of PEI-AuNRs by confocal imaging: Cells were cultured on 35 mm petri dishes for 24 h and treated with 50 μM PEI-AuNRs for 1, 3, 6, 12, 24 h. Cells were then washed by PBS and incubated separately for 30 min in cell culture medium with a mitochondrial marker (Mito Tracker, oxidized, Invitrogen) or a lysosome marker (Lyso Tracker, Invitrogen). After the medium was removed, cells were washed with PBS and fresh cell culture medium was added. The stained cells were observed by laser scanning microscopy (Olympus BX61W1 with Fluoview FV1000 software, Japan) with a 60X water immersion objective lens at 543 nm excitation and 560 nm emission. The light source was then switched to the near-infrared range and excitation signals were detected in the green color light channel, which was used to observe and image cells at 780 nm using a two photon laser (Maitai, Spectra Physics in USA). Finally, the Mito Tracker, Lyso Tracker (red fluorescence) and AuNRs (green fluorescence) images were merged by using Image J software (National Institutes of Health, USA).

Dark-field imaging to observe the cellular uptake: A549 and 16HBE cells were seeded on glass-bottom dishes for 24 h to allow the cells to attach to the surface of the wells. Final concentrations of 50 μM AuNRs were added to the cells and co-incubated for 3 and 12 h. Then the cells were washed with PBS three times and fixed with formalin for 30 min. The light scattering images were recorded using an inverted fluorescence microscope (Nikon Eclipse Ti–S, Nikon Instruments Inc., USA) observed with a highly numerical dark field condenser. An oil objective was used to collect only the scattered light from the samples.

Supporting Information

Supporting Information is available from the Wiley Online Library or from the author.

Acknowledgements
We thank Dr. Caixiang Liu, Lingling Xu, Yinglu Ji and Jinglong Tang for technical assistance in the experiments. This work was supported by grants from the National Basic Research Program of China (Grants 2012CB934004) and the National Natural Science Foundation of China (21175149, 91439102 and 21375144).

Received: February 11, 2016
Revised: May 19, 2016
Published online:

[1] I. Lynch, K. A. Dawson, *Nano Today* **2008**, *3*, 40.
[2] X. H. Huang, S. Neretina, M. A. El-Sayed, *Adv. Mater.* **2009**, *21*, 4880.
[3] L. Vigderman, B. P. Khanal, E. R. Zubarev, *Adv. Mater.* **2012**, *24*, 4811.
[4] L. Wang, X. Lin, J. Wang, Z. Hu, Y. Ji, S. Hou, Y. Zhao, X. Wu, C. Chen, *Adv. Funct. Mater.* **2014**, *24*, 4229.
[5] Y. Qiu, Y. Liu, L. Wang, L. Xu, R. Bai, Y. Ji, X. Wu, Y. Zhao, Y. Li, C. Chen, *Biomaterials* **2010**, *31*, 7606.
[6] A. S. Karakoti, S. Das, S. Thevuthasan, S. Seal, *Angew. Chem. Int. Edit.* **2011**, *50*, 1980.
[7] W. S. Cho, M. J. Cho, J. Jeong, M. Choi, H. Y. Cho, B. S. Han, S. H. Kim, H. O. Kim, Y. T. Lim, B. H. Chung, J. Jeong, *Toxicol. Appl. Pharm.* **2009**, *236*, 16.
[8] B. Kim, G. Han, B. J. Toley, C. K. Kim, V. M. Rotello, N. S. Forbes, *Nat. Nanotechnol.* **2010**, *5*, 465.
[9] S. B. Jin, X. W. Ma, H. L. Ma, K. Y. Zheng, J. Liu, S. Hou, J. Meng, P. C. Wang, X. C. Wu, X. J. Liang, *Nanoscale* **2013**, *5*, 143.
[10] T. S. Hauck, A. A. Ghazani, W. C. W. Chan, *Small* **2008**, *4*, 153.
[11] C. S. Rejiya, J. Kumar, V. Raji, M. Vibin, A. Abraham, *Pharmacol. Res.* **2012**, *65*, 261.
[12] Y. Lee, S. H. Lee, J. S. Kim, A. Maruyama, X. Chen, T. G. Park, *J. Control. Release* **2011**, *155*, 3.
[13] L. Xu, Y. Liu, Z. Chen, W. Li, Y. Liu, L. Wang, Y. Liu, X. Wu, Y. Ji, Y. Zhao, L. Ma, Y. Shao, C. Chen, *Nano Lett.* **2012**, *12*, 2003.
[14] T. Zhou, M. Yu, B. Zhang, L. Wang, X. Wu, H. Zhou, Y. Du, J. Hao, Y. Tu, C. Chen, T. Wei, *Adv. Funct. Mater.* **2014**, *24*, 6922.
[15] V. Serpooshan, M. Mahmoudi, M. M. Zhao, K. Wei, S. Sivanesan, K. Motamedchaboki, A. V. Malkovskiy, A. B. Goldstone, J. E. Cohen, P. C. Yang, J. Rajadas, D. Bernstein, Y. J. Woo, P. Ruiz-Lozano, *Adv. Funct. Mater.* **2015**, *25*, 4379.
[16] J. Li, C. Huang, D. Zheng, Y. Wang, Z. Yuan, *J. Proteome Res.* **2012**, *11*, 4654.
[17] L. M. Raamsdonk, B. Teusink, D. Broadhurst, N. S. Zhang, A. Hayes, M. C. Walsh, J. A. Berden, K. M. Brindle, D. B. Kell, J. J. Rowland, H. V. Westerhoff, K. van Dam, S. G. Oliver, *Nat. Biotechnol.* **2001**, *19*, 45.
[18] L. Zhang, L. Wang, Y. Hu, Z. Liu, Y. Tian, X. Wu, Y. Zhao, H. Tang, C. Chen, Y. Wang, *Biomaterials* **2013**, *34*, 7117.
[19] Y. P. Song, R. F. Zhao, Y. L. Hu, F. H. Hao, N. Li, G. J. Nie, H. R. Tang, Y. L. Wang, *J. Proteome Res.* **2015**, *14*, 5193.
[20] L. Wang, X. Jiang, Y. Ji, R. Bai, Y. Zhao, X. Wu, C. Chen, *Nanoscale* **2013**, *5*, 8384.
[21] L. Wang, Y. Liu, W. Li, X. Jiang, Y. Ji, X. Wu, L. Xu, Y. Qiu, K. Zhao, T. Wei, Y. Li, Y. Zhao, C. Chen, *Nano Lett.* **2011**, *11*, 772.
[22] S. P. Claus, T. M. Tsang, Y. L. Wang, O. Cloarec, E. Skordi, F. P. Martin, S. Rezzi, A. Ross, S. Kochhar, E. Holmes, J. K. Nicholson, *Mol. Syst. Biol.* **2008**, *4*, 1.
[23] T. W. M. Fan, A. N. Lane, *Prog. Nucl. Magn. Reson. Spectrosc.* **2008**, *52*, 69.
[24] J. Trygg, S. Wold, *J. Chemometr.* **2002**, *16*, 119.
[25] S. J. Roberts, A. J. Stewart, P. J. Sadler, C. Farquharson, *Biochem. J.* **2004**, *382*, 59.
[26] E. Frohlich, *Int. J. Nanomed.* **2012**, *7*, 5577.
[27] K. Glunde, Z. M. Bhujwalla, S. M. Ronen, *Nat. Rev. Cancer.* **2011**, *11*, 835.
[28] A. C. Hunter, *Adv. Drug. Del. Rev.* **2006**, *58*, 1523.
[29] S. M. Moghimi, P. Symonds, J. C. Murray, A. C. Hunter, G. Debska, A. Szewczyk, *Mol. Ther.* **2005**, *11*, 990.
[30] J.-P. Behr, *CHIMIA International Journal for Chemistry* **1997**, *51*, 34.
[31] S. Grande, A. Palma, A. M. Luciani, A. Rosi, L. Guidoni, V. Viti, *NMR Biomed.* **2011**, *24*, 68.

[32] K. Ohtsubo, J. D. Marth, *Cell* **2006**, *126*, 855.
[33] K. Sasai, Y. Ikeda, T. Fujii, T. Tsuda, N. Taniguchi, *Glycobiology* **2002**, *12*, 119.
[34] S. Banerjee, V. Sangwan, O. McGinn, R. Chugh, V. Dudeja, S. M. Vickers, A. K. Saluja, *J. Biol. Chem.* **2013**, *288*, 33927.
[35] M. R. Tosi, V. Tugnoli, G. Bottura, P. Lucchi, A. Battaglia, P. Giorgianni, *J. Mol. Struct.* **2001**, *565*, 323.
[36] H. Yokota, J. F. Guo, M. Matoba, K. Higashi, H. Tonami, Y. Nagao, *J. Magn. Reson. Imaging.* **2007**, *25*, 992.
[37] W. X. Chen, Y. K. Zu, Q. Huang, F. E. Chen, G. F. Wang, W. X. Lan, C. X. Bai, S. H. Lu, Y. Yue, F. Deng, *Magn. Reson. Med.* **2011**, *66*, 1531.
[38] F. Podo, *NMR Biomed.* **1999**, *12*, 413.
[39] H. Y. Jia, Y. Liu, X. J. Zhang, L. Han, L. B. Du, Q. Tian, Y. C. Xut, *J. Am. Chem. Soc.* **2009**, *131*, 40.
[40] P. Sestili, C. Fimognari, *Biomed. Res. Int.* **2015**, *2015*, 1.
[41] G. Waris, H. Ahsan, *J. Carcinog.* **2006**, *5*, 14.
[42] A. Gole, C. J. Murphy, *Chem. Mater.* **2005**, *17*, 1325.
[43] C. N. Xiao, F. H. Hao, X. R. Qin, Y. L. Wang, H. R. Tang, *Analyst* **2009**, *134*, 916.
[44] H. Dai, C. Xiao, H. Liu, F. Hao, H. Tang, *J. Proteome Res.* **2010**, *9*, 1565.
[45] L. Eriksson, J. Trygg, S. Wold, *J. Chemometr.* **2008**, *22*, 594.
[46] O. Cloarec, M. E. Dumas, A. Craig, R. H. Barton, J. Trygg, J. Hudson, C. Blancher, D. Gauguier, J. C. Lindon, E. Holmes, J. Nicholson, *Anal. Chem.* **2005**, *77*, 1282.
[47] Z. D. Xu, K. Harvey, T. Pavlina, G. Dutot, G. Zaloga, R. Siddiqui, *Lipids* **2010**, *45*, 199.
[48] H. D. Li, W. D. Zhu, L. K. Zhang, H. H. Lei, X. Y. Wu, L. Guo, X. W. Chen, Y. L. Wang, H. R. Tang, *Scientific Reports* **2015**, *5*, 1.

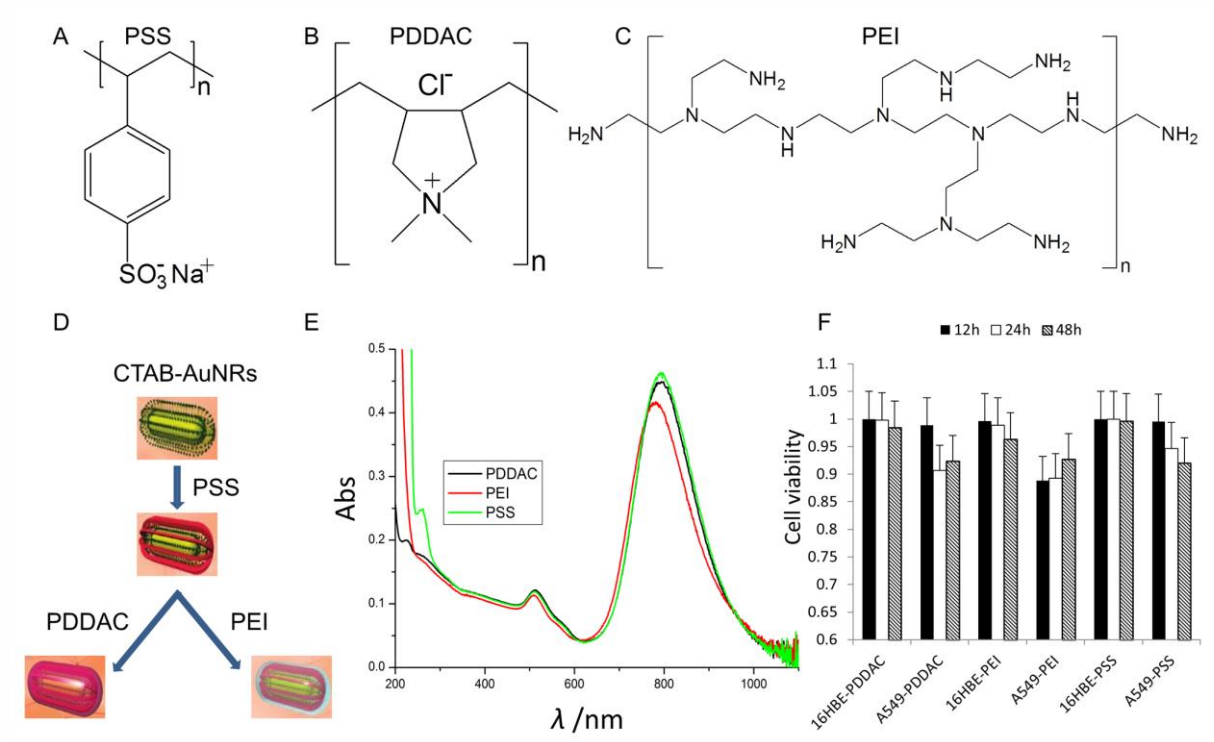


Figure 1. Illustration of formulation and characterization of different coated AuNRs. A-C: chemical structure of PSS, PDDAC and PEI, respectively. D: illustration of formulation of different coated AuNRs. E: UV-Vis-NIR extinction spectra of different coated AuNRs in de-ionized water. F: cell viability of exposure to AuNRs at 50 μM.

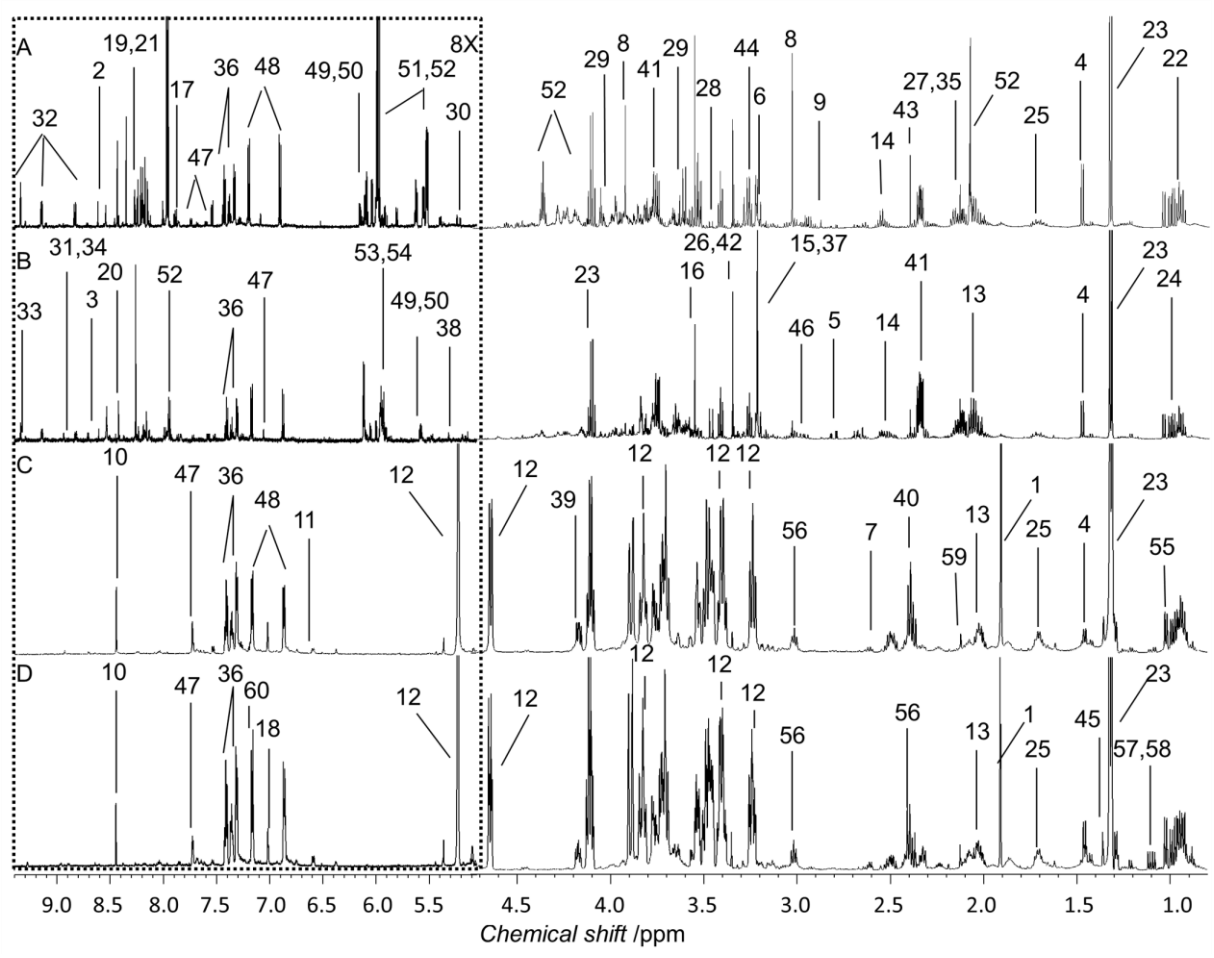


Figure 2. Representative 600 MHz ^{1}H NMR spectra of aqueous extracts from AuNRs treated 16HBE (A) and A549 (B) cells and cell culture media from 16HBE cell culture (C) and A549 cell culture (D). The region of 5.1 to 9.4 ppm in the spectra is vertically expanded 8 times compared to the region of 0.7 to 4.7 ppm. Key: 1. Acetate; 2. Adenosine diphosphate (ADP); 3. Adenosine monophosphate (AMP); 4. Alanine (Ala); 5. Aspartate (Asp); 6. Choline; 7. Citrate; 8. Creatine; 9. Dimethylamine (DMA); 10. Formate; 11. Fumarate; 12. Glucose (Glc); 13. Glutamate (Glu); 14. Glutamine; 15. Glycerolphosphocholine (GPC); 16. Glycine (Gly); 17. Guanosine; 18. Histidine (His); 19. Hypoxanthine; 20. Inosine; 21. Inosine-5'-monophosphate (5'-IMP); 22. Isoleucine (Ile); 23. Lactate; 24. Leucine (Leu); 25. Lysine (Lys); 26. Methanol; 27. Methionine (Met); 28. Monomethyl phosphate; 29. *Myo*-inositol; 30. *N*-acetyl-glucosamine (GlcNAc); 31. Nicotinamide; 32. Nicotinamide adenine dinucleotide

(NAD^+); 33. Nicotinamide adenine dinucleotide phosphate ($NADP^+$); 34. Nicotinuric acid; 35. Oxidized glutathione (GSSG); 36. Phenylalanine (Phe); 37. Phosphocholine (PCho); 38. Phosphoenol pyruvic acid (PEP); 39. Pyroglutamate; 40. Pyruvate; 41. Reduced glutathione (GSH); 42. *Scyllo*-inositol; 43. Succinate; 44. Taurine; 45. Threonine (Thr); 46. Trimethylamine (TMA); 47. Tryptophan (Trp); 48. Tyrosine (Tyr); 49. UDP Glucose (UDP-Glc); 50. UDP glucuronate (UDP-GlcA); 51. UDP-N-Acetyl galactosamine (UDP-GalNAc); 52. UDP-N-acetyl glucosamine (UDP-GlcNAc); 53. Uracil; 54. Uridine; 55. Valine (Val); 56. 2-Oxoglutarate (2-OG); 57. 2-Oxoisoleucine (2-O-Ile); 58. 2-Oxoisovalerate (2-O-Val); 59. 2-Oxoleucine (2-O-Leu); 60. 4-Hydroxyphenylpyruvate (4HPPA).

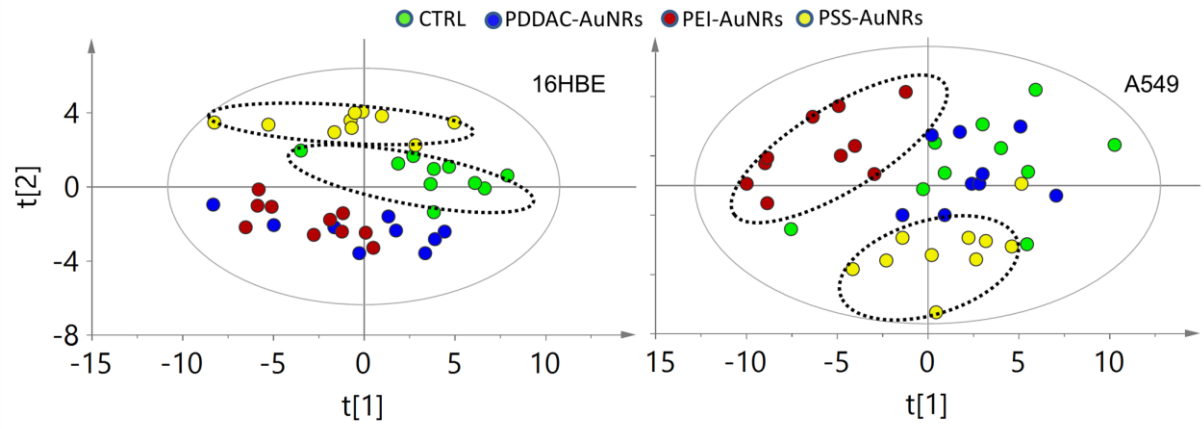


Figure 3. PCA analysis of NMR profiles obtained from different extracts of cells exposed to different AuNRs. In the plot, each dot represents NMR profiling data from an individual sample and colors indicate samples in different treatment groups. Negatively charged PSS-AuNRs treated group was clearly separated from positively charged AuNRs treated group. In A549 cells, PEI-AuNRs treated group was clearly separated from others.

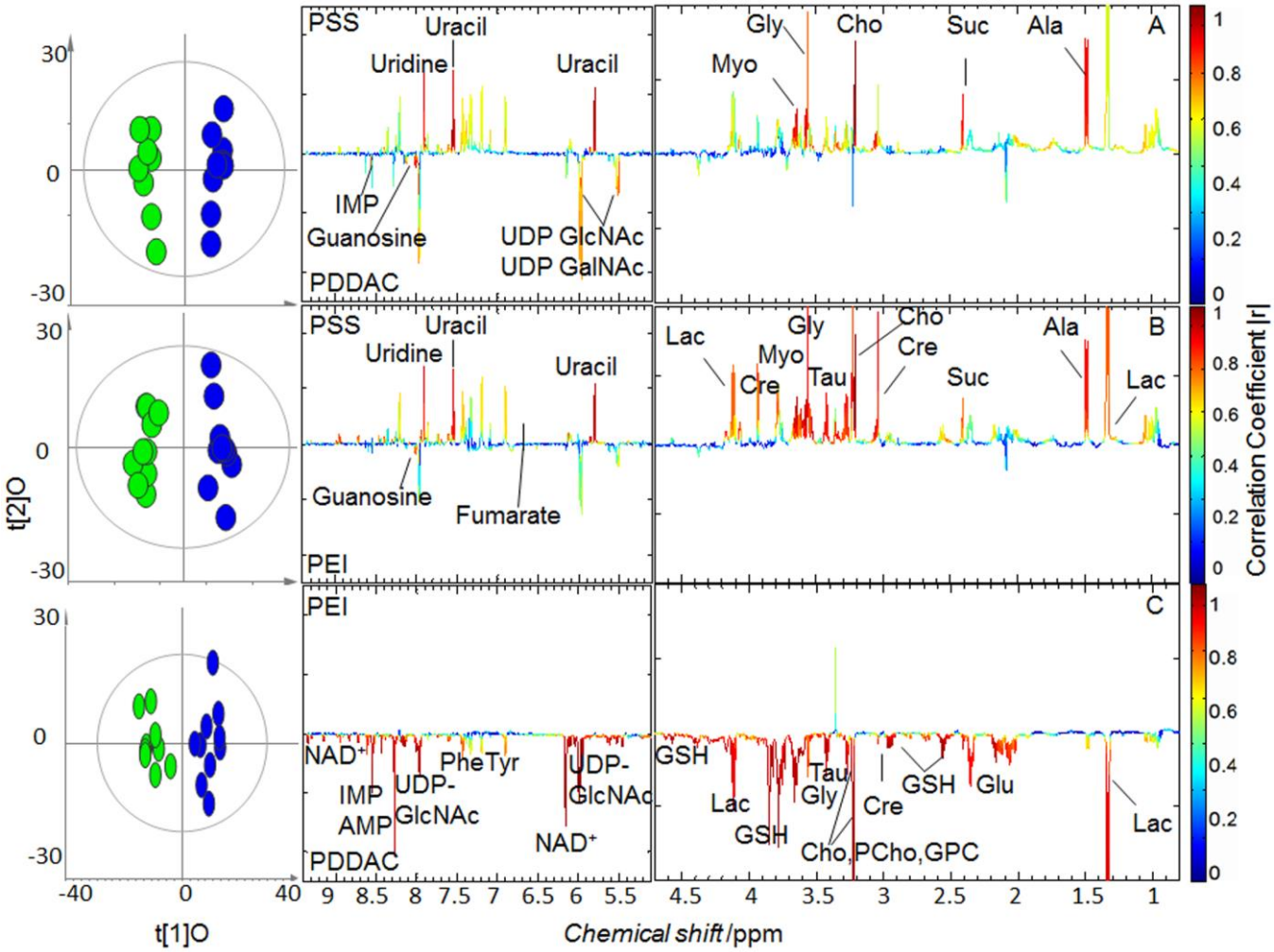


Figure 4. OPLS-DA score plot (left) and coefficient plot (right) showing the discrimination between negatively and positively charged AuNRs treated cells. A and B are from 16HBE cells; C is from A549 cells. In the score plot, each dot represents NMR profiling data from an individual sample and colors indicate samples in different treatment groups. In the coefficient plot, the signal pointing upward represents the metabolites content of the group labeled in the upper-left is higher than that in the group labeled in the lower left (for example, PSS and PDDAC for Figure 4 A). The absolute value of r was color coded to indicate the significance of metabolites alterations. The cutoff value of |r| is 0.602 (n=10, P<0.05). Ala: Alanine; Suc: Succinate; Cho: Choline; Myo: *Myo*-inositol; Cre: Creatine; Tau: Taurine; Gly: Glycine; Lac: Lactate; IMP: Inosine-5'-monophosphate; AMP: Adenosine monophosphate; NAD^+: Nicotinamide adenine dinucleotide; UDP-GlcNAc: Uridine diphosphate-N-Acetyl

glucosamine; Phe: Phenylalanine; Tyr: Tyrosine; Glu: Glutamate; PCho: Phosphocholine; GSH: Glutathione; GPC: Glycerolphosphocholine.

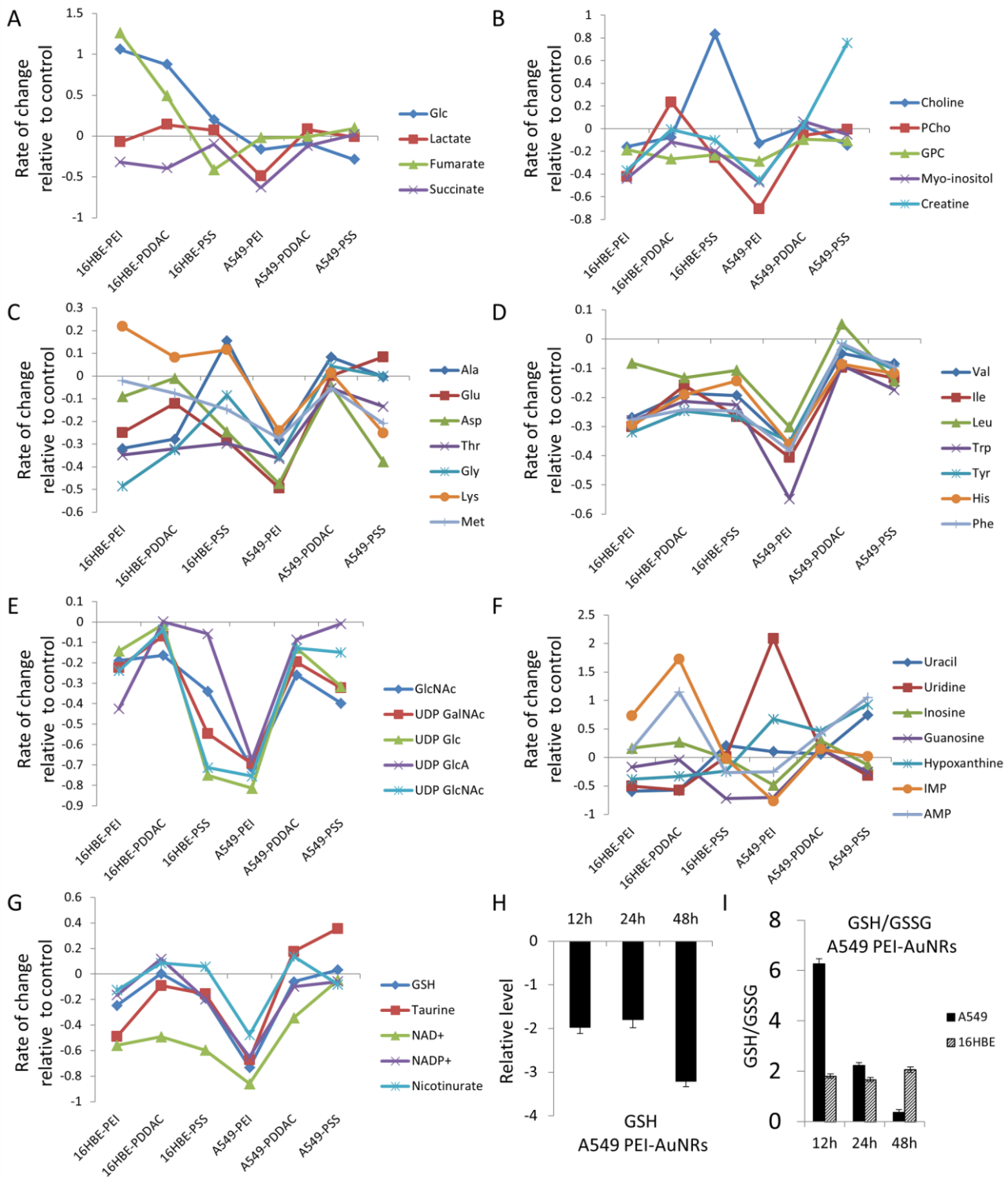


Figure 5. Altered metabolites in treated cells relative to those of the untreated cells collected at 12 h of exposure to AuNRs (A-G), GSH concentration measured by NMR (H) and ratio of GSH/GSSG (I).

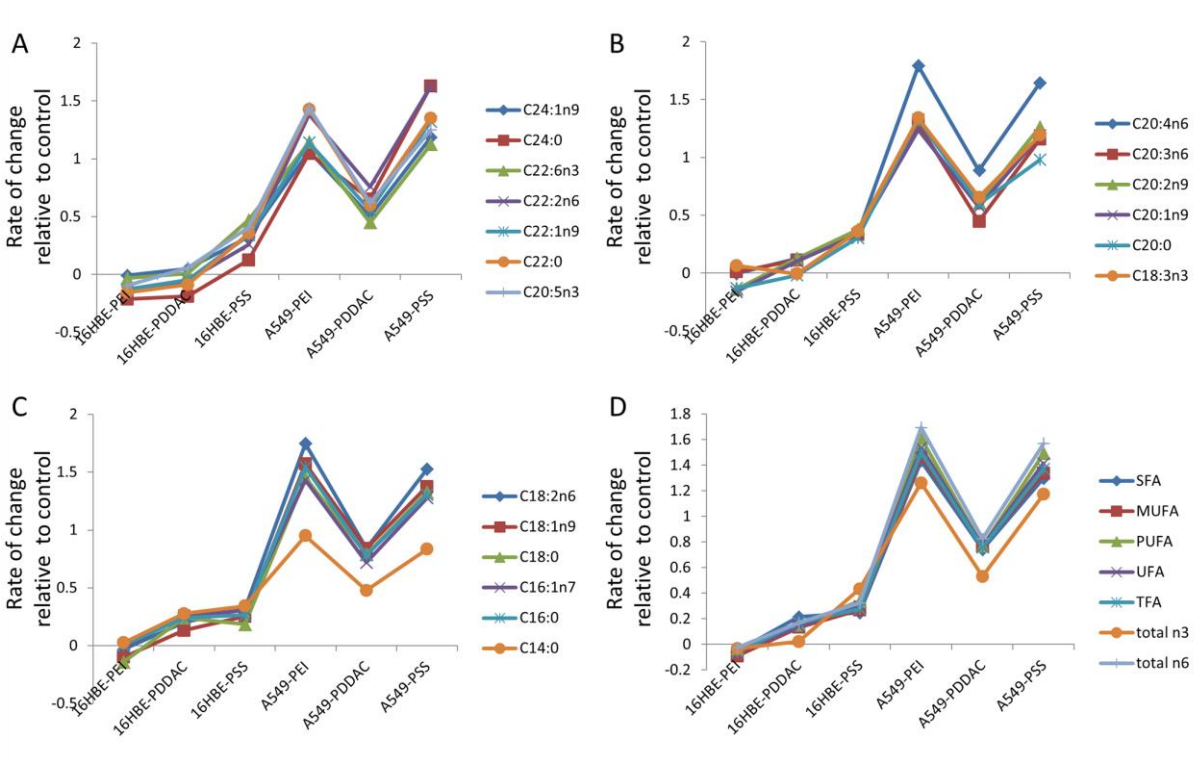


Figure 6. Relative changes of fatty acid concentrations from the cells exposed to AuNRs and the untreated cells.

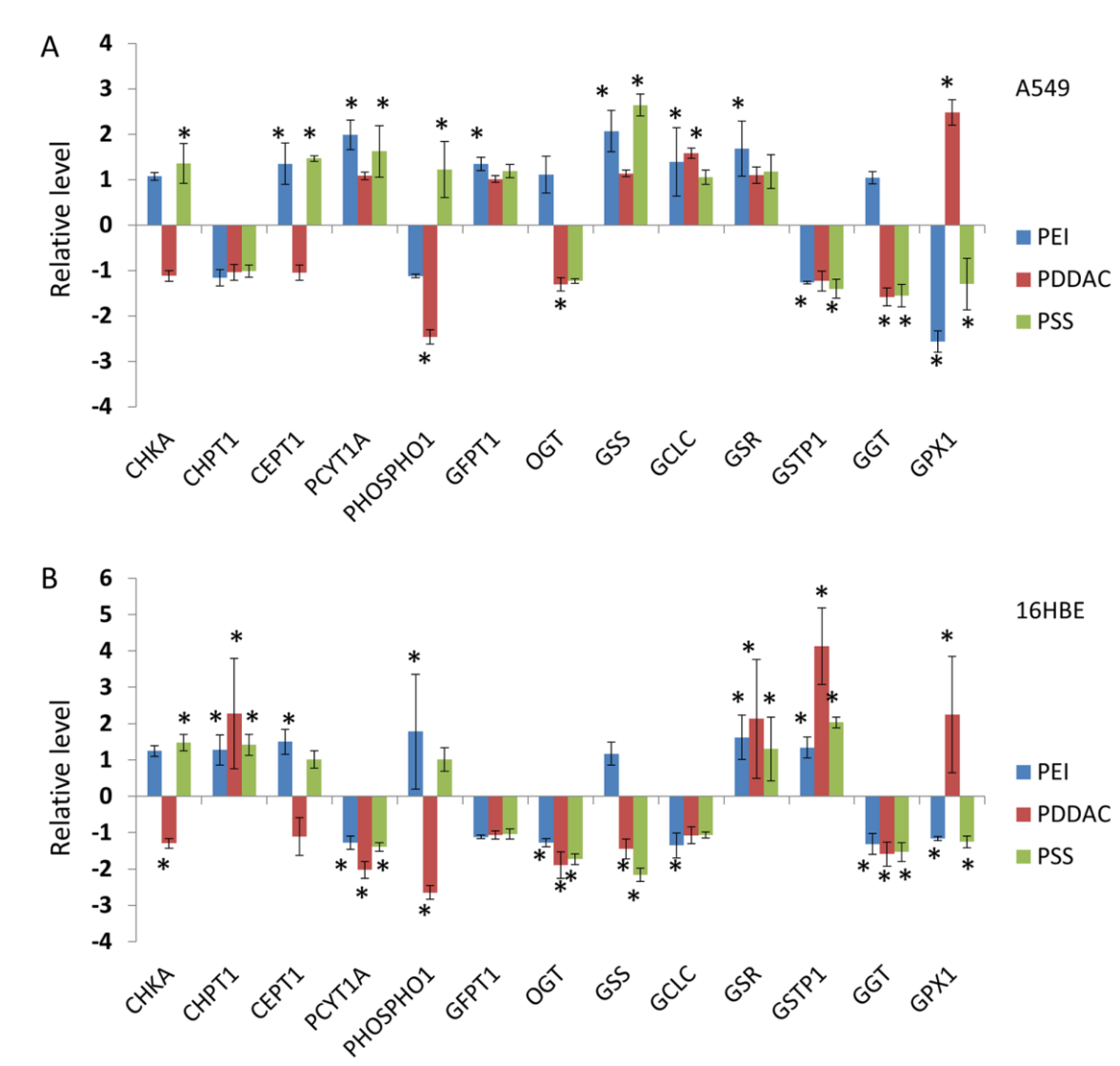


Figure 7. Relative transcriptional levels of certain genes from the cells exposed to AuNRs and the untreated cells. A: A549 cells; B:16HBE cells.

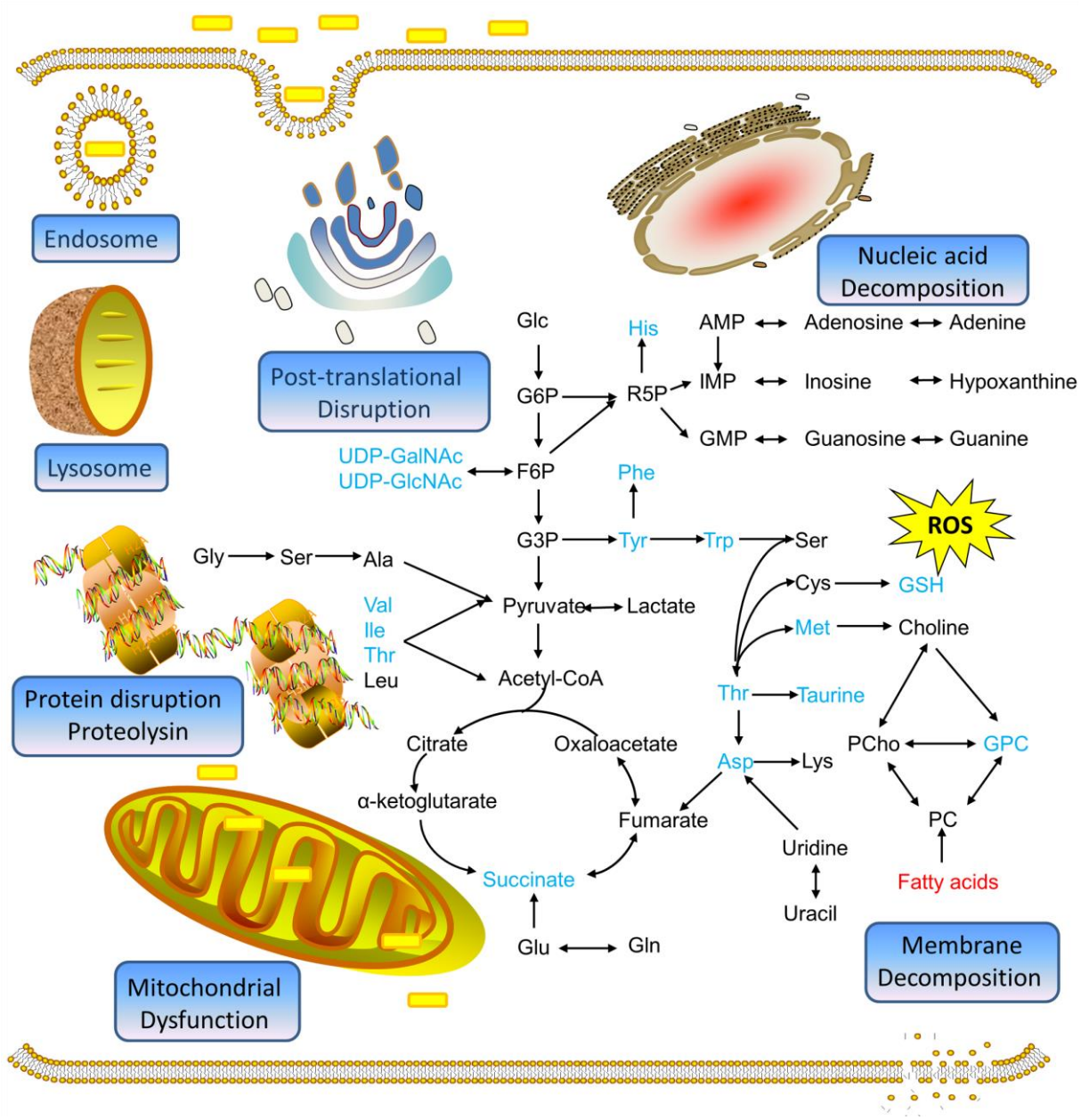


Figure 8. Summary of the main systemic effects of different coated AuNRs induced to 16HBE and A549 cells.

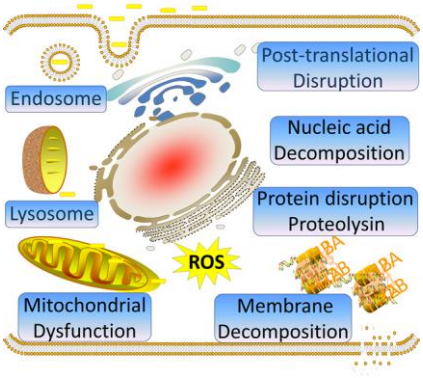
Table of contents

Different surface modified AuNRs induced distinct metabolic consequences to A549 and 16HBE cells. PEI-AuNRs showed specific cytotoxiciy to A549 cells companied with large disruptions to the cell metabolisms. These AuNRs caused a disruption in the intracellular environment that affects energy metabolism, as well as targeted choline metabolism, disrupted the hexosamine biosynthesis pathway and induced oxidative stress to cells.

Keywords: Gold Nanorods; Metabolomics; Biomedical Applications; Surface Modification; Cancer Cell

Zhigang Liu, Liming Wang, Limin Zhang, Xiaochun Wu, Guangjun Nie, Chunying Chen, Huiru Tang, Yulan Wang**

Metabolic characteristics of 16HBE and A549 cells exposed to different surface modified gold nanorods



Copyright WILEY-VCH Verlag GmbH & Co. KGaA, 69469 Weinheim, Germany, 2013.

Supporting Information

Metabolic characteristics of 16HBE and A549 cells exposed to different surface modified gold nanorods

Zhigang Liu, Liming Wang, Limin Zhang, Xiaochun Wu, Guangjun Nie, Chunying Chen, Huiru Tang, Yulan Wang**

Table S1. Metabolites assigned from NMR data.

Key	Metabolites	Assignment	δ^1H (multiplicity[a])	δ^{13}C	Sample[b]
1	Acetate	CH_3	1.92(s)	26.2	C,M
		COOH		184.2	
2	Adenosine diphosphate (ADP)	CH-ring	8.54(s)	142.4	C
		CH-ring	8.27(s)	155.9	
		C1H-ribose	6.14(d)	89.9	
		C2H-ribose	4.61(m)	72.8	
		C3H-ribose	4.51(m)	73.1	
		C4H-ribose	4.38(m)	86.8	
		C5H-ribose	4.01(m)	66.2	
3	Adenosine monophosphate (AMP)	2-H	8.61(s)	147.2	C
		8-H	8.27(s)	146.5	
		2-H'	6.15(d)	90.1	
4	Alanine (Ala)	CH_3	1.48(d)	19.2	C,M
		CH	3.78(q)	53.2	
		COOH		178.8	
5	Aspartate	β-CH_2	2.69(m)	39.2	C,M
		β-CH_2'	2.82(dd)	39.2	
		α-CH	3.90(m)	51.8	
		β-COOH		180.5	
		α-COOH		176.9	
6	Choline	$N(CH_3)_3$	3.21(s)	57.1	C
		NCH_2	3.54(m)	58.5	
		OCH_2	4.05(m)	72.4	
7	Citrate	CH_2	2.53(dd)	48.9	M
		CH_2'	2.69(dd)	48.9	
		C3		77.6	
		C1,5		180.9	
		C6		182.8	

8	Creatine	CH_3	3.04(s)	40	C
		CH_2	3.93(s)	57.3	
		C=NH		159.4	
		COOH		177.2	
9	Dimethylamine (DMA)	CH_3	2.76(s)	32.5	C
10	Formate	H-CO	8.46(s)		C,M
11	Fumarate	CH	6.52(s)	138.2	C,M
12	Glucose (Glc)	CH_2	5.24(d)	95.5	C,M
		CH	4.65(d)	99.3	
			3.25(t)	77.5	
			3.39-3.55(m)		
			3.69-3.93(m)		
13	Glutamate (Glu)	β-CH_2	2.12(m)	30.1	C,M
		β-CH_2'	2.07(m)	30.1	
		γ-CH_2	2.36(m)	36.8	
		α-CH	3.77(m)	57.6	
		C=O		183.6	
		COOH		177.5	
14	Glutamine	α-CH	2.14(m)	26.1	C
		β-CH_2	2.44(m)	33.4	
		γ-CH_2	3.77(m)	57.1	
15	Glycerolphosphocholine (GPC)	N-CH_3	3.23(s)	56.7	C
		1-CH_2	3.60(dd)		
		2-CH	3.89(m)		
		3-CH_2	3.72(dd)		
		α-CH_2	4.32(t)		
		β-CH_2	3.68(t)		
16	Glycine (Gly)	CH_2	3.56(s)	44.5	C
		COOH		175.3	
17	Guanosine	CH-ring	8.01(s)	140.9	C
		C1H, ribose	5.92(d)	91.7	
		C3H, ribose	4.41(dd)	73.4	
		C4H, ribose	4.24(dt)	88.2	
		C5H, ribose	3.84(m)	64	
18	Histidine (His)	β-CH_2	3.14(dd)	30.7	C,M
		β-CH_2'	3.25(dd)	30.7	
		α-CH	3.99(dd)	57.6	
		5-CH	7.08(s)	120.3	
		3-CH	7.84(s)	140.2	
		C-ring		133.6	
		COOH		176.4	
19	Hypoxanthine	C1H	8.20(s)	149.4	C

		C2H	8.21(s)	145.8	
20	Inosine	CH_2	3.84(dd)	64.2	C
		CH_2'	3.92(dd)	63.8	
		5-H'	4.29(dd)	87.1	
		4-H'	4.44(dd)	73.7	
		3-H’	4.78(t)	74.6	
		2-H'	6.10(d)	91.3	
		8-H	8.24(s)	150.4	
		2-H	8.35(s)	144.5	
21	Inosine-5'-monophosphate (5'-IMP)	2-H	8.54(s)	144.5	C
		8-H	8.19 (s)	146.8	
		2-H'	6.15(d)	89.5	
22	Isoleucine (Ile)	δ-CH_3	0.94(t)	14.2	C,M
		γ-CH_3	1.01(d)	17.7	
		γ-CH_2	1.27(m)	27.6	
		γ-CH_2'	1.48(m)	27.6	
		β-CH	1.99(m)	38.8	
		α-CH	3.67(m)	64.6	
		COOH		177.1	
23	Lactate	CH_3	1.33(d)	22.9	C,M
		CH	4.11(q)	72.1	
		COOH		185.3	
24	Leucine (Leu)	δ-CH_3	0.96(d)	24.5	C,M
		δ-CH_3'	0.97(d)	23.5	
		γ-CH	1.69(m)	27.3	
		β-CH_2	1.71(m)	42.8	
		α-CH	3.74(t)	56.4	
		COOH		178.3	
25	Lysine (Lys)	γ-CH_2	1.48(m)	25.3	C,M
		δ-CH_2	1.72(m)	28.9	
		β-CH_2	1.91(m)	33.1	
		ε-CH_2	3.03(t)	42.2	
		α-CH	3.76(t)	57.6	
		COOH		177.5	
26	Methanol	CH_3	3.36(s)	52.1	C,M
27	Methionine (Met)	α-H	3.86(t)	56.8	C
		β-H	2.16(m)	32.7	
		γ-H	2.65(t)	31.6	
		CH_3	2.14(s)	16.6	
28	Monomethyl phosphate	CH_3	3.47(d)	54.2	C

29	*Myo*-inositol	C4H	3.53(dd)	74.7	C
		C1H	3.62(t)	75.8	
		C2H	4.06(t)	75.6	
		C3H	3.28(t)	77.7	
30	N-acetyl-glucosamine (GlcNAc)	α-C1H	5.21(d)	93.66	C
		α-C2,5,6H	3.85 (m)	73.46	
		α-C3H	3.76	72.72	
		α-C4H	3.46	97.78	
		β-C1H	4.71	59.51	
		β-C2H	3.67	76.73	
		β-C3H	3.53	72.72	
		β-C4,5H	3.46	24.75	
		NA-H	2.05 (s)		
31	Nicotinamide	2-CH	8.94(d)	152.6	C,M
		6-CH	8.73(dd)	155.6	
		4-CH	8.25(d)	144.5	
		5-CH	7.61(dd)	134.7	
32	Nicotinamide adenine dinucleotide (NAD^+)	N5-ring	8.19(dd)	132.2	C
		N4-ring	8.83(d)	149.8	
		N2-ring	9.34(s)	143.5	
		N6-ring	9.15(d)	146.2	
		A2H-ring	8.01(s)	126	
		A8H-ring	8.43(s)	143.3	
		A1H	6.09(d)	102.9	
		A1H'	5.99(d)	91.2	
33	Nicotinamide adenine dinucleotide phosphate ($NADP^+$)	N5-ring	8.14(dd)	132.2	C
		N4-ring	8.82(d)	149.8	
		N2-ring	9.30(s)	143.5	
		N6-ring	9.10(d)	146.2	
		A8H-ring	8.42(s)	143.3	
		A1H	6.11(d)	102.9	
		A1H'	6.04(d)	91.2	
34	Nicotinuric acid	N2-ring	8.95(s)	149.9	C
		N4-ring	8.72(d)	154.3	
		N5-ring	8.26(m)	139.3	
		N6-ring	7.60(dd)	127.1	
		CH_2	4.01(s)	46.6	
35	Oxidized glutathione (GSSG)	CH_2	2.17(m)	29.8	C
		CH_2'	2.53(m)	34	
		S-CH_2	2.98(dd)	57.2	

		S-CH_2'	3.30(dd)	57.2	
		N-CH	3.78(m)	45.3	
		CH	4.76(q)	55.3	
36	Phenylalanine (Phe)	β-CH_2	3.13(dd)	39.4	C,M
		β-CH_2'	3.21(dd)	39.4	
		α-CH	3.98(dd)	57.5	
		2,6-CH	7.33(m)	132.7	
		4-CH	7.38(m)	133	
		3,5-CH	7.43(m)	132.8	
		C-ring		139.4	
		COOH		176.4	
37	Phosphocholine (PCho)	N-CH_2	3.22(s)	56.7	C
		β-CH_2	4.17(m)	69.5	
		α-CH_2	3.60(m)		
38	Phosphoenol pyruvic acid (PEP)	CH	5.27(d)	100.5	C
39	Pyroglutamate	5-CH	4.18(m)	61.6	M
		4-CH_2	2.51/2.04(m)	28.4	
		3-CH_2	2.41(m)	32.6	
		COOH		183.5	
		C=O		184.6	
40	Pyruvate	β-CH_3	2.38(s)		M
41	Reduced glutathione (GSH)	CH_2	2.17(m)	29.6	C
		CH_2'	2.55(m)	35	
		S-CH_2	2.95(dd)	28.3	
		N-CH	3.78(m)	46.7	
		CH	4.57(q)	54.7	
42	Scyllo-inositol	CH	3.35(s)	77.1	C
43	Succinate	CH_2	2.41(s)	36.6	C,M
		COOH		185.4	
44	Taurine	S-CH_2	3.26(t)	51	C
		N-CH_2	3.42(t)	38.9	
45	Threonine (Thr)	γ-CH_3	1.33(d)	22.7	C,M
		α-CH	3.59(d)	63.8	
		β-CH	4.26(m)	68.8	
		COOH		175.8	
46	Trimethylamine (TMA)	CH_3	2.88(s)	47.8	C
47	Tryptophan (Trp)	C4H-ring	7.74(d)	121.8	C,M
		C5H-ring	7.20(t)	119.6	
		C6H-ring	7.29(t)	120.8	
		C7H-ring	7.54(d)	114.1	
		C2H-ring	7.33(s)	126.3	

		α-CH	4.05(m)	58.7	
		β-CH_2	3.32(m)	28.8	
		β-CH_2'	3.49(m)	28.8	
48	Tyrosine (Tyr)	β-CH_2	3.06(dd)	38.8	C,M
		β-CH_2'	3.15(dd)	38.8	
		α-CH	3.94(dd)	57.5	
		3,5-CH	6.90(d)	119.5	
		2,6-CH	7.20(d)	134.8	
		COOH		177.1	
49	UDP Glucose (UDP-Glc)	C1H', ribose	5.99(d)	91.3	C
		C5-ring	5.98(d)	105.4	
		C6-ring	7.96(d)	144.4	
		C5H', ribose	4.26(m)	67.8	
		G1-H	5.61(m)	98.7	
50	UDP glucuronate (UDP-GlcA)	C6-ring	7.95(d)	144.5	C
		C1H', ribose	6.00(d)	91.4	
		C5-ring	5.98(d)	105.4	
		G1-H	5.62(m)	98.1	
51	UDP-N-Acetyl galactosamine (UDP-GalNAc)	NA-H	2.09(s)	24.9	C
		G1-H	5.55(d)	97.4	
		C1H', ribose	5.99(d)	91.1	
		C5-ring	5.97(d)	105.4	
		C6-ring	7.96(d)	144.1	
		C5H', ribose	4.25(m)	67.8	
		C4H', ribose	4.29(m)	85.9	
52	UDP-N-acetyl glucosamine (UDP-GlcNAc)	C6-ring	7.96(d)	145.5	C
		C1H'-ribose	5.99(d)	92	
		C5-ring	5.97(d)	106.3	
		C3H', ribose	4.37(m)	73.3	
		C5H', ribose	3.99(m)	72.1	
		C4H', ribose	4.24(m)	89.2	
		G1-H	5.52(dd)	97.9	
		G2-H	3.93(m)	56.9	
		G3-H	3.83(m)	74.4	
		G4-H	3.56(dd)	74.5	
		NA-H	2.08(s)	24.9	
		NA-C=O		177.4	
53	Uracil	CH	5.81(d)	102.3	C,M
		CH'	7.54(d)	146.5	
		C=O		170.6	
		C=O		155.9	
54	Uridine	CH_2	3.81(d)	64.1	C

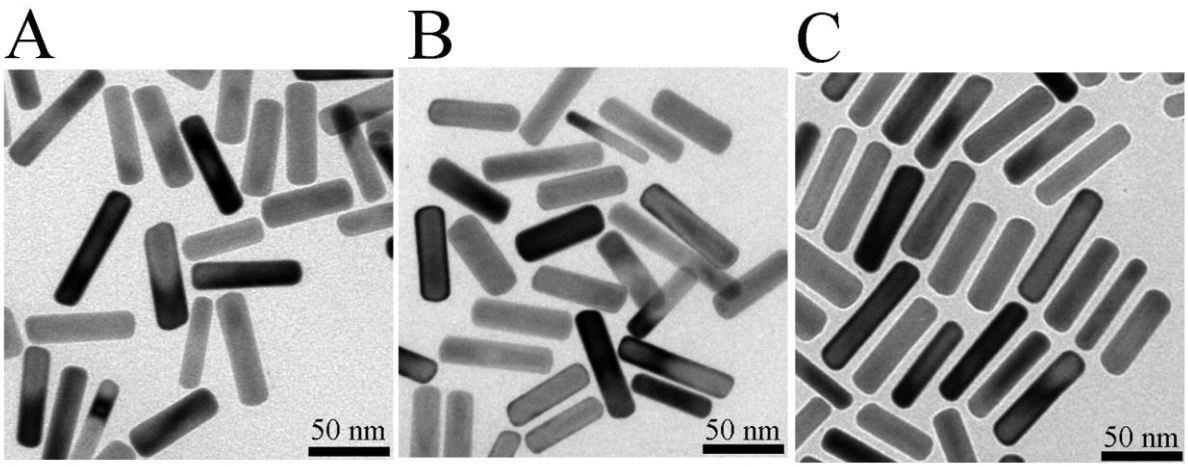
		CH_2'	3.92(d)	64.1	
		4-H'	4.11(q)	87.1	
		3-H'	4.24(t)	73.4	
		2-H'	4.38(t)	77.2	
		5-H	5.90(d)	105.6	
		6-H	5.92(d)	92.6	
		1-H'	7.88(d)	145.3	
55	Valine (Val)	γ-CH_3	0.99(d)	19.9	C,M
		γ-CH_3'	1.04(d)	20.9	
		β-CH	2.27(m)	32	
		α-CH	3.61(d)	63.6	
		COOH		177.1	
56	2-Oxoglutarate (2-OG)	β-CH_2	3.01(t)	39	M
		γ-CH_2'	2.45(t)	33.7	
		2-C		207.8	
57	2-Oxoisoleucine (2-O-Ile)	α-CH_3	1.10(d)	16.7	M
		γ-CH_3	0.89(t)	13.6	
		CH	2.94(m)	46.7	
		CH_2	1.70/1.45(m)	27.4	
58	2-Oxoisovalerate (2-O-Val)	CH_3	1.12(d)	19.4	M
		CH	3.02(m)	39.9	
59	2-Oxoleucine (2-O-Leu)	CH_3	0.94(d)	24.4	M
		CH_2	2.62(d)	51.2	
		CH	2.12(m)	30.1	
60	4-Hydroxyphenylpyruvate (4HPPA)	CH	7.18(d)	134	M
		CH'	6.85(d)	118.9	
		CH_2	4.01(s)		

a: Multiplicity: singlet (s), doublet (d), triplet (t), quartet (q), doublet of doublets (dd), doublet of triplets (dt), multiplet (m).
b: Sample: C: cell extracts; M: cell culture media.

Table S2. Primers of mRNA

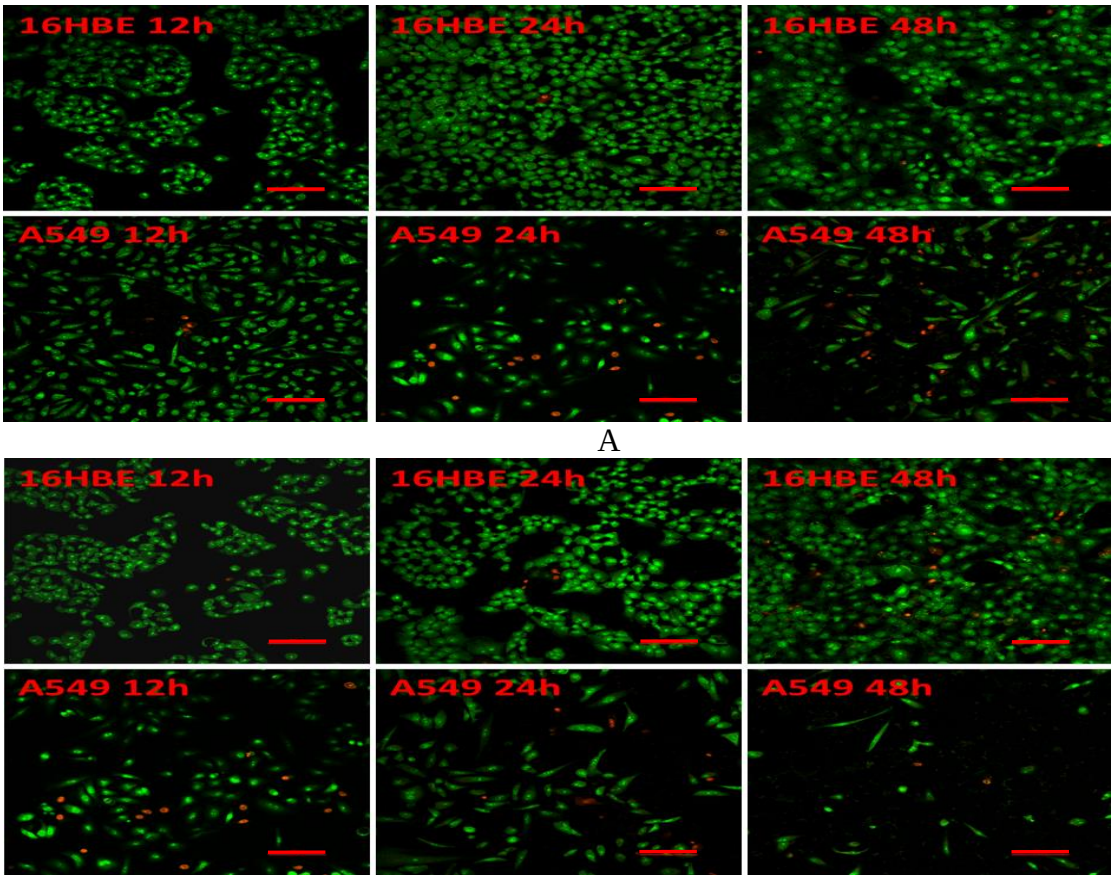
Genes		Primers
CHKA	F	CGCCGAGAAAATGGCTACAT
	R	CAGTTCCAAGGGCAGATTGT
CHKB	F	CAGCCATTGCCACGAAGATG
	R	CATCTCAGGGAGGCCAGTTG
CHPT1	F	GCTCGTGCTCATCTCCTACTG
	R	CTTCTGGCTTGTTTCCCATCA
CEPT1	F	GGGTGTACTTGTTGGGGTCA
	R	CGATGCCCACTCATGGATCTT
PHOSPHO1	F	CCCTTCCCCACTTCTTACACT
	R	CAGCCACTCATTGTCGGT
PCYTIA	F	AACGGGGCAACAGAAGAAGAT
	R	AGGTCGCTCACAAGGAGTTC
GCLM	F	GGCACAGGTAAAACCAAATAGTAAC
	R	CAAATTGTTTAGCAAATGCAGTCA
GSS	F	TTGACCAGCGTGCCATAGAG
	R	ATCCACAAACAGCCTTCGGT
GCLC	F	TCCAGGTGACATTCCAAGCC
	R	CACTCCCCAGCGACAATCAA
GFPT1	F	ATCTCTCTCGTGTGGACAGC
	R	TGACGCGATTGGTGTGTTCTA
GFPT2	F	ACTGTGCTCCAAGGACGATAC
	R	TGGGGAAGTCAACGTCATATCC
OGT	F	CAGCACAGAACCAACGAAAC
	R	CTGCCTCAAAATCTCCTGCCT
GAPDH	F	CTTTGGTATCGTGGAAGGACT
	R	AGAGGCAGGGATGATGTTCT
GSR	F	TCACGCAGTTACCAAAAGGAAA
	R	TTCATCACACCCAAGTCCCTG
GSTP1	F	CAATACCATCCTGCGTCACCT
	R	ATCCTTGCCCGCCTCATAGT
GGT1	F	TGTTGTGTGTGGGGCTCAT
	R	CTTTTCGTGTGGTGCTGTTGT
GPX1	F	GGACTACACCCAGATGAACG
	R	TCTCCTGATGCCCAAACTG

Figure S1. TEM images for size and shape of Au NRs.



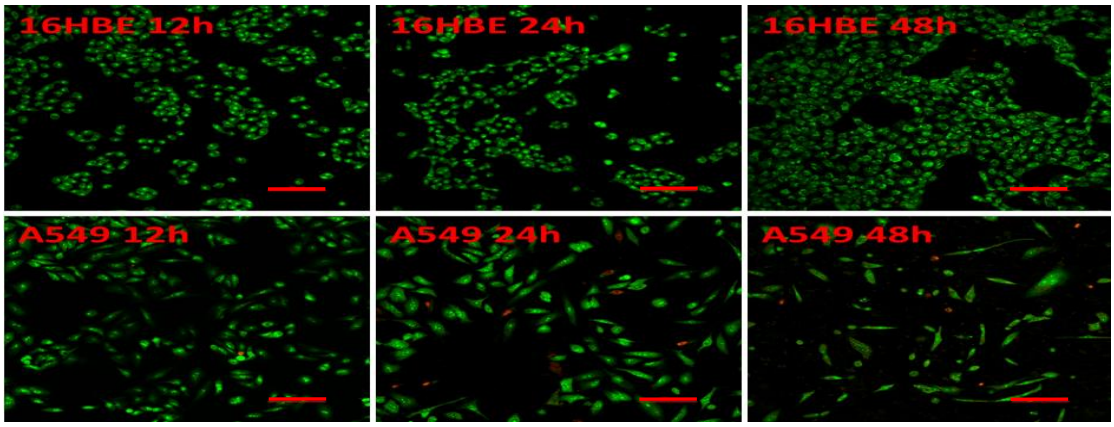
A: PEI-AuNRs; B: PDDAC-AuNRs; C; PSS-AuNRs

Figure S2. Fluorescent imaging for A549 and 16HBE cells treated with different coated AuNRs for 12 h, 24 h and 48 h. Fluorescent imaging shows the Live-Dead staining for live cells (green color) and dead cells (red color). A for PDDAC treated cells; B for PEI treated cells; C for PSS treated cells. The scale bar is 100 μm.



A

B



C

Figure S3. Localization of PEI-AuNRs in 16HBE cells with lysosome staining

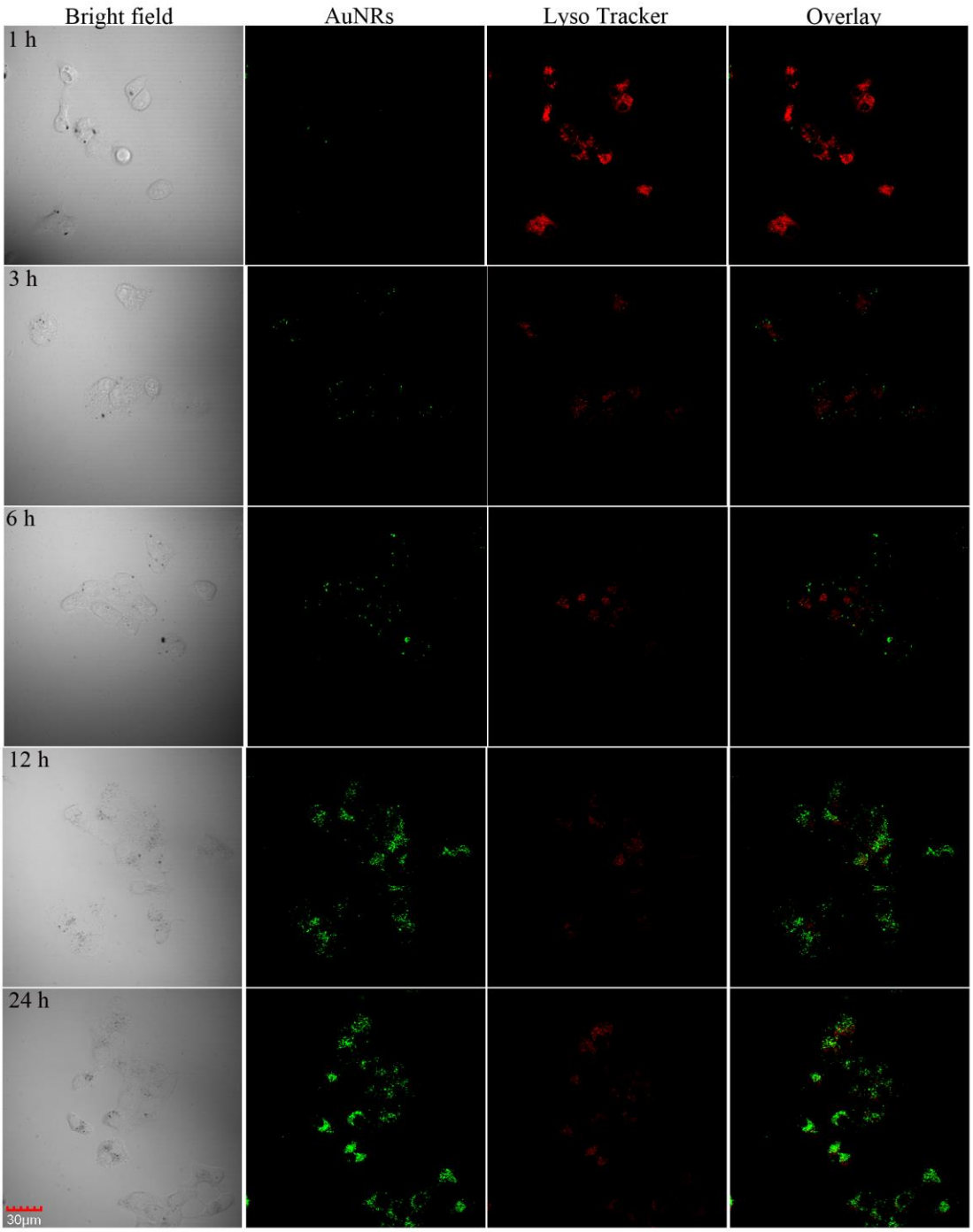


Figure S4. Localization of PEI-AuNRs in 16HBE cells with mitochondria staining

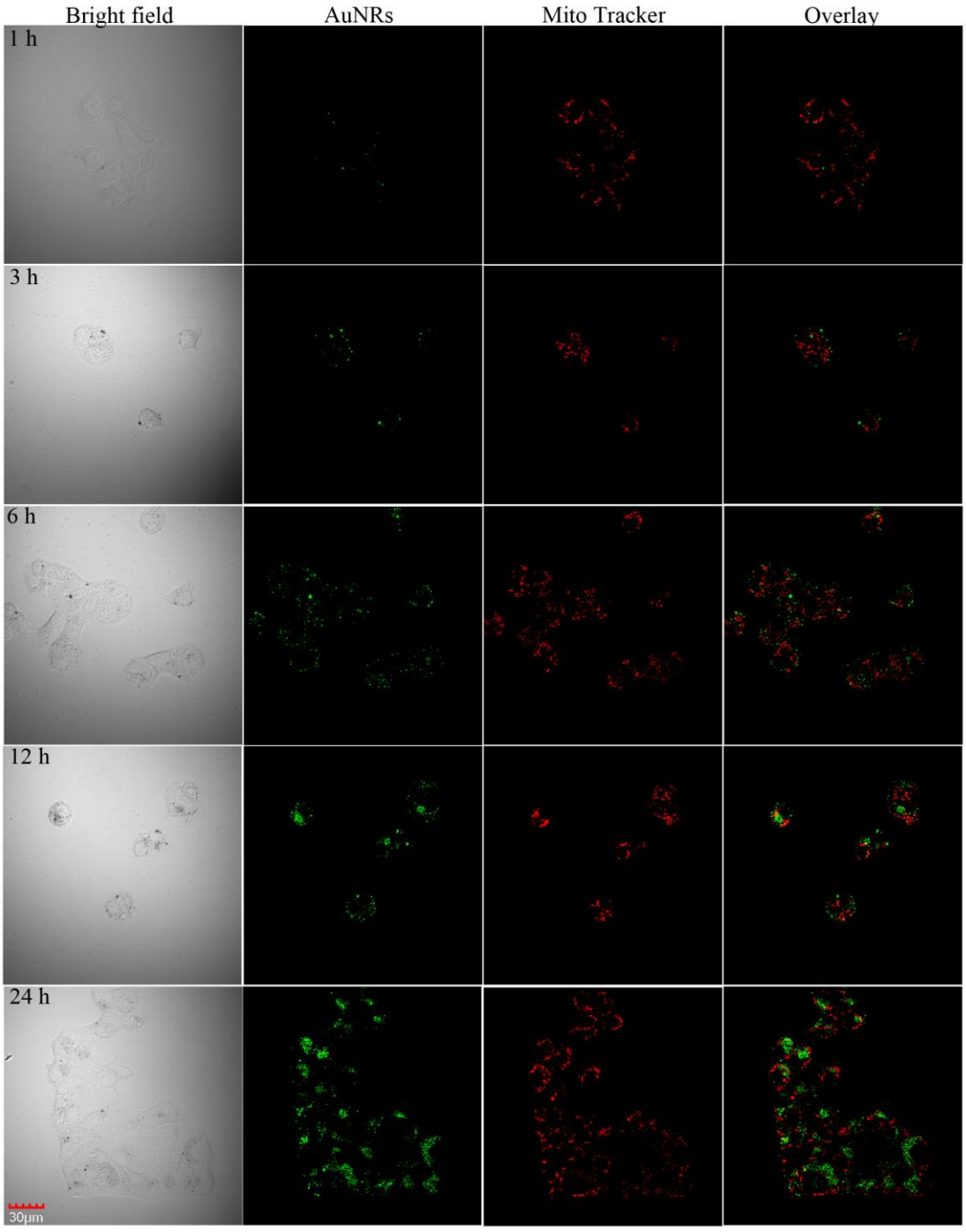


Figure S5. Localization of PEI-AuNRs in A549 cells with lysosome staining

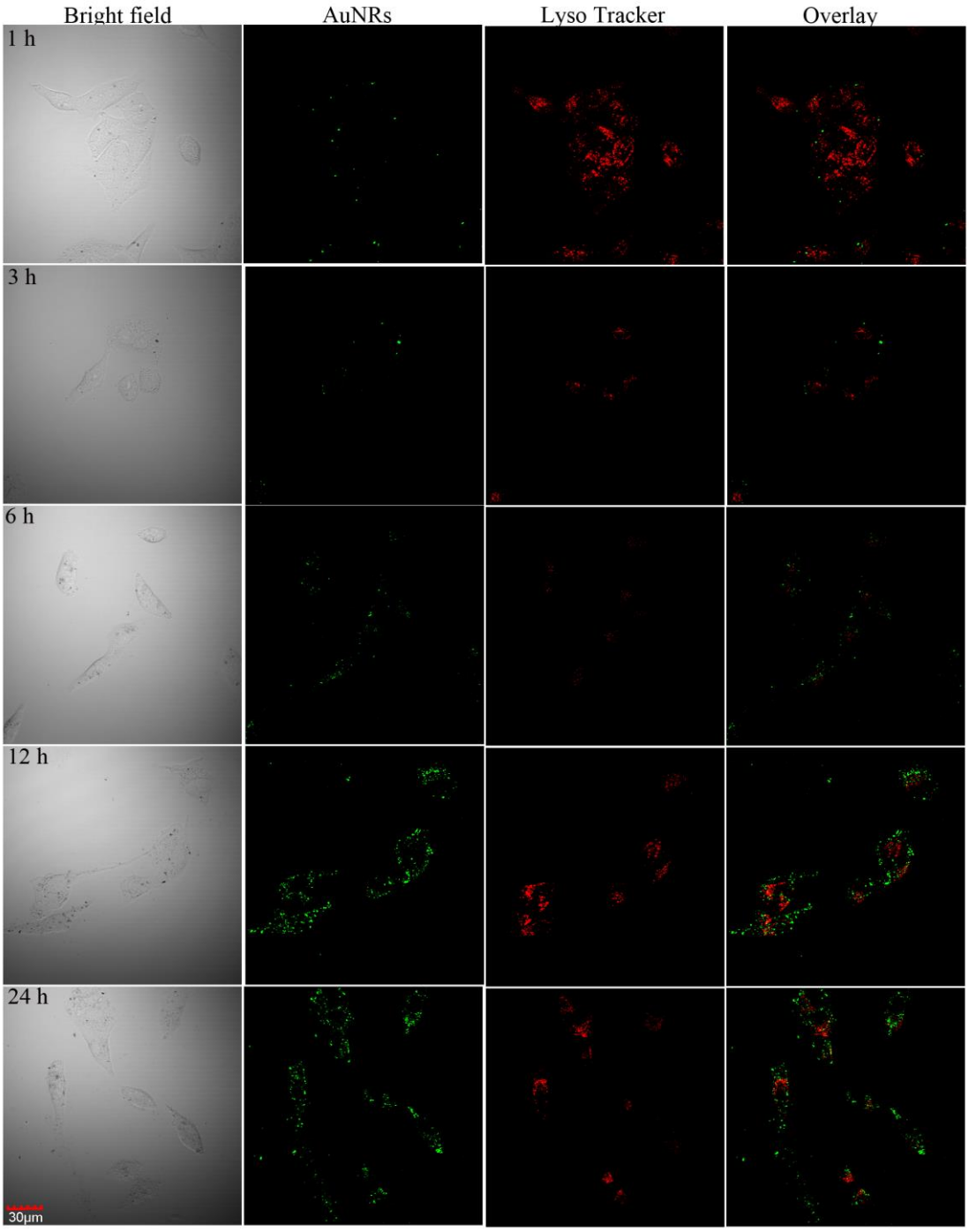


Figure S6. Localization of PEI-AuNRs in A549 cells with mitochondria staining

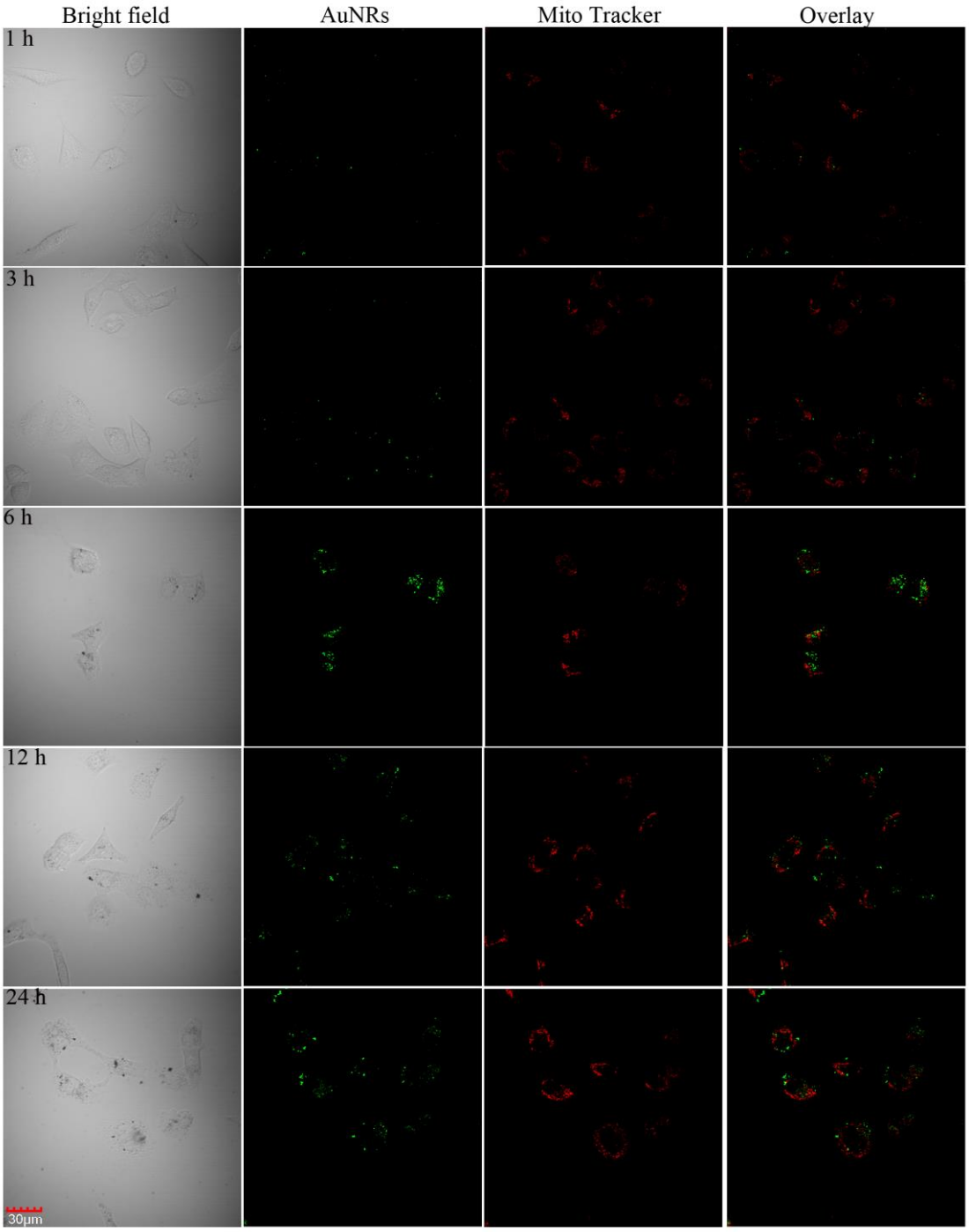


Figure S7. Cellular uptake of PEI-AuNRs by dark-field microscopy

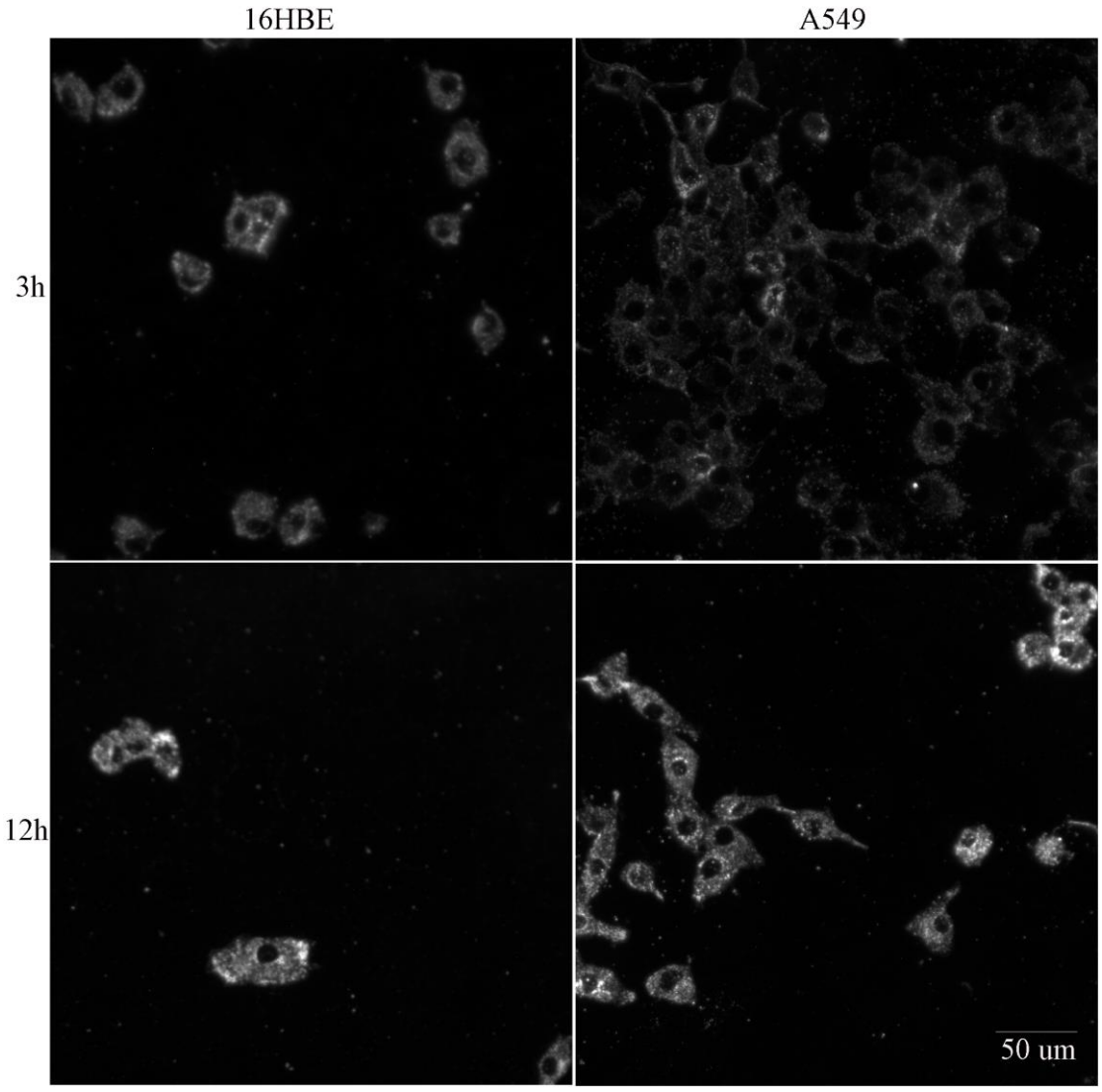


Figure S8. Heatmap of all changed metabolites. The metabolites colored in red or blue represent that they are significantly up or down regulated in the AuNRs treated group.

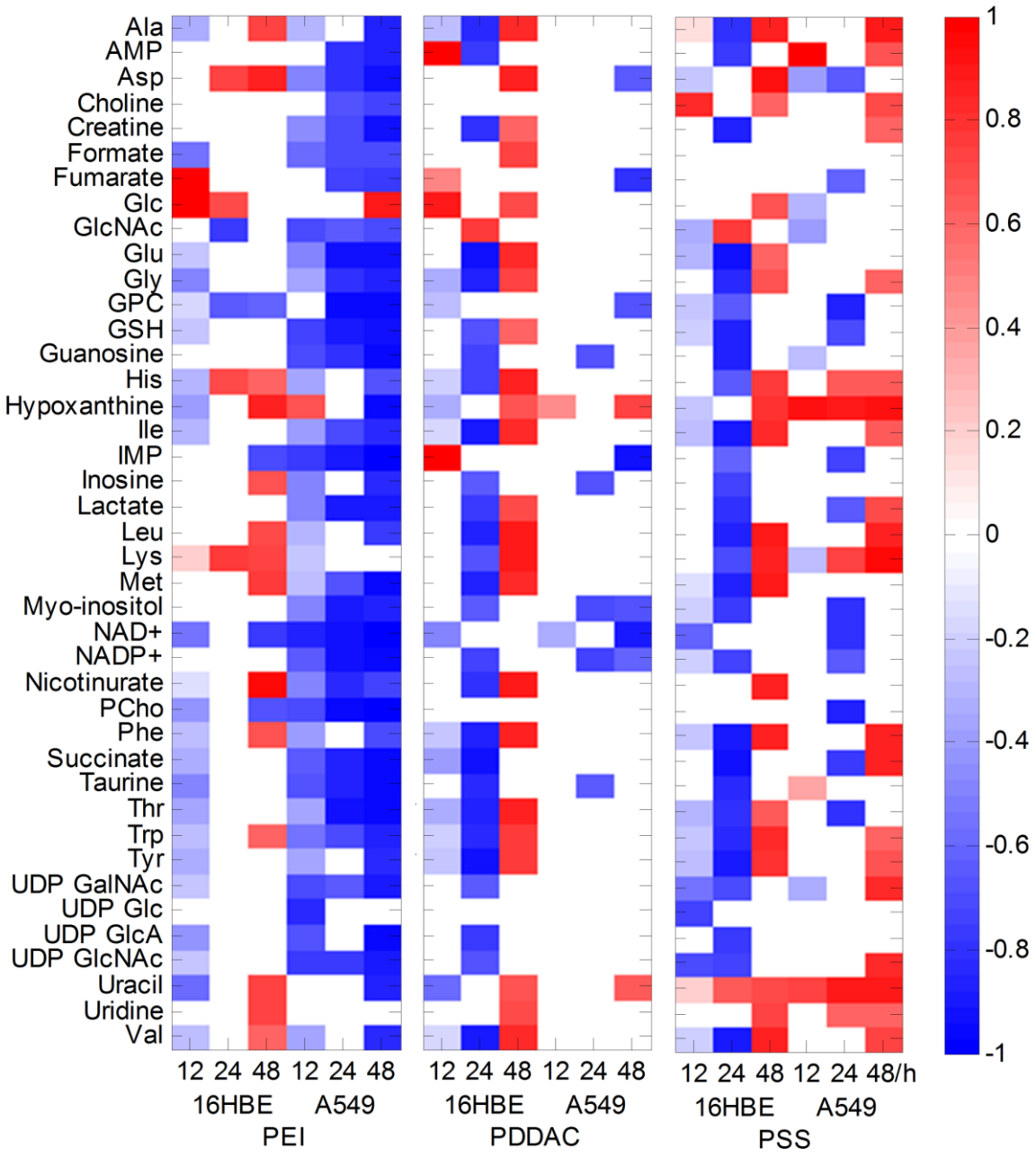


Figure S9. Heatmap of all changed metabolites in cell culture media. The metabolites colored in red or blue represent that they are significantly up or down regulated in the AuNRs treated group.

